Bulletin of the Seismological Society of America, Vol. 106, No. 3, pp. 881–903, June 2016, doi: 10.1785/0120150166

Ⓔ

Late Holocene Liquefaction at Sites of Contemporary Liquefaction during the 2010–2011 Canterbury Earthquake Sequence, New Zealand

by Sarah H. Bastin, Kari Bassett, Mark C. Quigley,* Brett Maurer, Russell A. Green, Brendon Bradley, and David Jacobson

Abstract The 2010–2011 Canterbury earthquake sequence (CES) caused up to 10 episodes of liquefaction at highly susceptible sites in eastern Canterbury, resulting in severe damage to land and infrastructure. Subsurface investigations at five sites over two study areas revealed CES dikes and sills that align with and crosscut pre-CES liquefaction features, including dikes, a lateral sill, a sandblister, and a buried compound sandblow. Crosscutting relationships combined with carbon-14 (^{14}C) dating constrain the timing of the pre-CES liquefaction features to likely post-A.D. 1321 and pre-1960 in one study area. Pre-CES features in the second study area likely formed in three distinct episodes: post-A.D. 1458 and possibly during the 1901 Cheviot earthquake, between A.D. 1297 and 1901, and pre-A.D. 1458. The liquefaction potential of known active faults within the wider Canterbury region are evaluated from back-calculated magnitude-bound curves and peak ground acceleration (PGA) approximated using a New Zealand-specific ground-motion prediction equation and compared with global liquefaction triggering thresholds. Analysis indicates that many active faults within North Canterbury and offshore that are within 50 km of the study sites and capable of triggering $M_w > 6.5$ earthquakes have the potential to cause widespread liquefaction. Ruptures of these faults may have formed the pre-CES liquefaction features. Combining the backcalculation approach with the modeled PGA proves effective in determining the active faults capable of triggering liquefaction at the study sites and are therefore capable of triggering liquefaction in the future.

Online Material: Overview and further discussion of the probabilistic magnitude-bound methodology framework and derivative curves, description of sediment units, and table of peak ground acceleration (PGA).

Introduction

Earthquake-induced cyclic shearing may trigger deformation in loosely consolidated and saturated sediment, causing pore-water pressures to increase in the affected media. Liquefaction may occur as pore-water pressures exceed the initial vertical confining stresses causing the breakdown of the grain arrangement (Seed and Idriss, 1982; Idriss and Boulanger, 2008). Pore-water and liquefied sediment may be ejected to the ground surface through subsurface dikes, or it may be injected into the near surface as lateral sills, stalled dikes, and/or injection features (Sims and Garvin, 1995; Obermeier, 1996; Tuttle and Barstow, 1996; Tuttle and Hartleb, 2012; Quigley *et al.*, 2013). Liquefaction ejecta typically manifests at the surface as sandblows, fissures, surface flooding, and localized vertical (i.e., subsidence) and/or horizontal (i.e., lateral-spreading) ground movement (Seed and Idriss, 1982; Obermeier, 1996; Tuttle and Barstow, 1996; Cubrinovski *et al.*, 2010; Tuttle and Hartleb, 2012; Quigley *et al.*, 2013). The surficial features are susceptible to erosion or reworking into surrounding sediments by aeolian and/or fluvial action and therefore may be removed from or obscured in the geologic record (Sims and Garvin, 1995; Reid *et al.*, 2012; Quigley *et al.*, 2013). Subsurface liquefaction features are commonly preserved in the geologic record where host

*Now at School of Earth Sciences, The University of Melbourne, Victoria 3010, Australia.

sediments are preserved and are termed "paleoliquefaction" (Obermeier, 1996; Tuttle, 2001; Obermeier *et al.*, 2005).

Paleoliquefaction provides evidence for paleoearthquake shaking that exceeded the threshold value for liquefaction (Green *et al.*, 2005). Analysis of paleoliquefaction features enables recurrence intervals, ground motions, and magnitudes of paleoearthquakes to be estimated (Obermeier, 1996; Tuttle *et al.*, 2002; Green *et al.*, 2005; Tuttle and Atkinson, 2010). Site-specific peak ground acceleration (PGA) may be back-calculated for historic earthquakes and/or ruptures of known active faults using ground-motion prediction equations (GMPEs). Comparison of modeled PGA with liquefaction-triggering thresholds enables faults capable of triggering liquefaction to be identified. Recent compilations of earthquake and liquefaction data suggest a liquefaction-inducing threshold of magnitude normalized PGA ($PGA_{7.5} = 0.09g$) earthquake (Santucci de Magistris *et al.*, 2013), although minor liquefaction has been reported in highly susceptible sediments under $PGA_{7.5}$ as low as $\sim 0.06g$ (Quigley *et al.*, 2013). Magnitude-bound curves, which correlate earthquake magnitude with the maximum site-to-source distance of observed liquefaction, are also widely applied in paleoliquefaction studies. The curves constrain the distribution of rupture locations and magnitudes that have the potential for inducing liquefaction at a given site (Obermeier, 1998; Tuttle, 2001; Olson *et al.*, 2005; Papathanassiou *et al.*, 2005; Pirrotta *et al.*, 2007). A methodology for backcalculating magnitude-bound curves has been proposed by Maurer *et al.* (2015). This methodology identifies the range of possible earthquake sources capable of triggering liquefaction at a site with paleoliquefaction.

The 2010–2011 Canterbury earthquake sequence (CES) caused repeated episodes of liquefaction in parts of eastern Christchurch and in the northern township of Kaiapoi, New Zealand (Fig. 1; Cubrinovski *et al.*, 2010; Wotherspoon *et al.*, 2012; Quigley *et al.*, 2013). Severe liquefaction-induced damage to land and infrastructure recurred during the September 2010 M_w 7.1 Darfield earthquake, and the subsequent February 2011 M_w 6.2 Christchurch, June 2011 M_w 6.0, and December 2011 M_w 5.9 earthquakes and resulted in the central government purchase of upward of 6000 residential properties (Cubrinovski *et al.*, 2010, 2011; Parker and Steenkamp, 2012; Quigley *et al.*, 2013). The record of historic earthquakes in the wider Christchurch area is limited to post-European settlement of the area in 1843. Historic reports indicate that five damaging earthquakes occurred within the Canterbury region prior to the CES and between 1869 and 1922 (Pettinga *et al.*, 2001; Downes and Yetton, 2012). The 1901 $M_w \sim 6.9$ Cheviot event caused widespread damage within the Canterbury area and triggered liquefaction in Kaiapoi (Fig. 1; Berrill *et al.*, 1994). The 1922 M_w 6.4 Motunau, North Canterbury, 1888 $M_w \sim 7.2$ Hope fault, 1870 $M_w \sim 5.7$ Lake Ellesmere, and 1869 $M_w \sim 4.8$ Christchurch earthquakes also caused widespread damage in the wider Christchurch region (Elder *et al.*, 1991; Stirling *et al.*, 1999; Pettinga *et al.*, 2001; Downes and Yetton, 2012). Additional prehistoric earthquakes known to have affected the Canterbury region include the 1717 $M_w \sim 8.1$ Alpine fault (Sutherland *et al.*, 2007) and the ~1400–1500 $M_w \sim 7.2$ Porters Pass earthquakes (Howard *et al.*, 2005). No liquefaction was reported nor has been identified in Christchurch following any of these events or in Kaiapoi following events other than the 1901 earthquake (Berrill *et al.*, 1994; Downes and Yetton, 2012). Understanding the approximate timing, location, and magnitude of liquefaction-inducing prehistoric earthquakes within the Canterbury region is therefore important in informing future land-use planning decisions and may contribute to seismic-hazard modeling (Stirling *et al.*, 2012).

In this study, we present new stratigraphic and chronologic evidence for pre-CES liquefaction at three sites within eastern Christchurch and two sites in Kaiapoi, with the goal of further constraining the timing of previous liquefaction-inducing earthquakes within the Canterbury region. The potential that ruptures of known active faults will trigger liquefaction at the study sites is also evaluated from (1) PGA approximated using a New Zealand-specific GMPE and compared with liquefaction triggering thresholds and (2) back-calculated magnitude-bound curves.

Geologic Setting

The eastern Canterbury region is situated upon a low-relief and low-elevation alluvial landscape (0–20 m above sea level [m.a.s.l.]) along the eastern margin of the Canterbury Plains (Fig. 1). The region is predominantly underlain by drained peat swamps, fluvial sands and silts, and estuarine, dune, and foreshore sands (Fig. 1; Brown and Weeber, 1992; Forsyth *et al.*, 2008). The western Canterbury region is primarily underlain by fluvial gravel, sand, and silt deposited by the Waimakariri River during its avulsion across the Canterbury Plains and subsequent overbank flow (Cowie, 1957; Brown and Weeber, 1992).

The sediments in eastern Canterbury were deposited during shoreline progradation and marine regression following the mid-Holocene highstand with shorelines recorded up to 8 km inland from the location of the modern shoreline at ~6500 yr B.P. (Brown and Weeber, 1992). Fluvial sands and silts comprise reworked deposits of the braided Waimakariri River and transported by the meandering rivers (i.e., Avon and Kaiapoi Rivers; Fig. 1) that regularly avulsed across the region prior to European settlement (Cowie, 1957; Brown and Weeber, 1992). The youthful and unconsolidated nature of the fine sands to silts combined with high water tables (1–2 m depth) and localized artesian water pressures pose a long-recognized high-liquefaction hazard (Elder *et al.*, 1991; Brown and Weeber, 1992; Christchurch Engineering Lifelines Group, 1997; Clough, 2005).

Avondale Study Area

The study area of Avondale, eastern Christchurch, experienced severe liquefaction-induced damage during the CES (Fig. 1). The southern extent of the suburb is situated adjacent

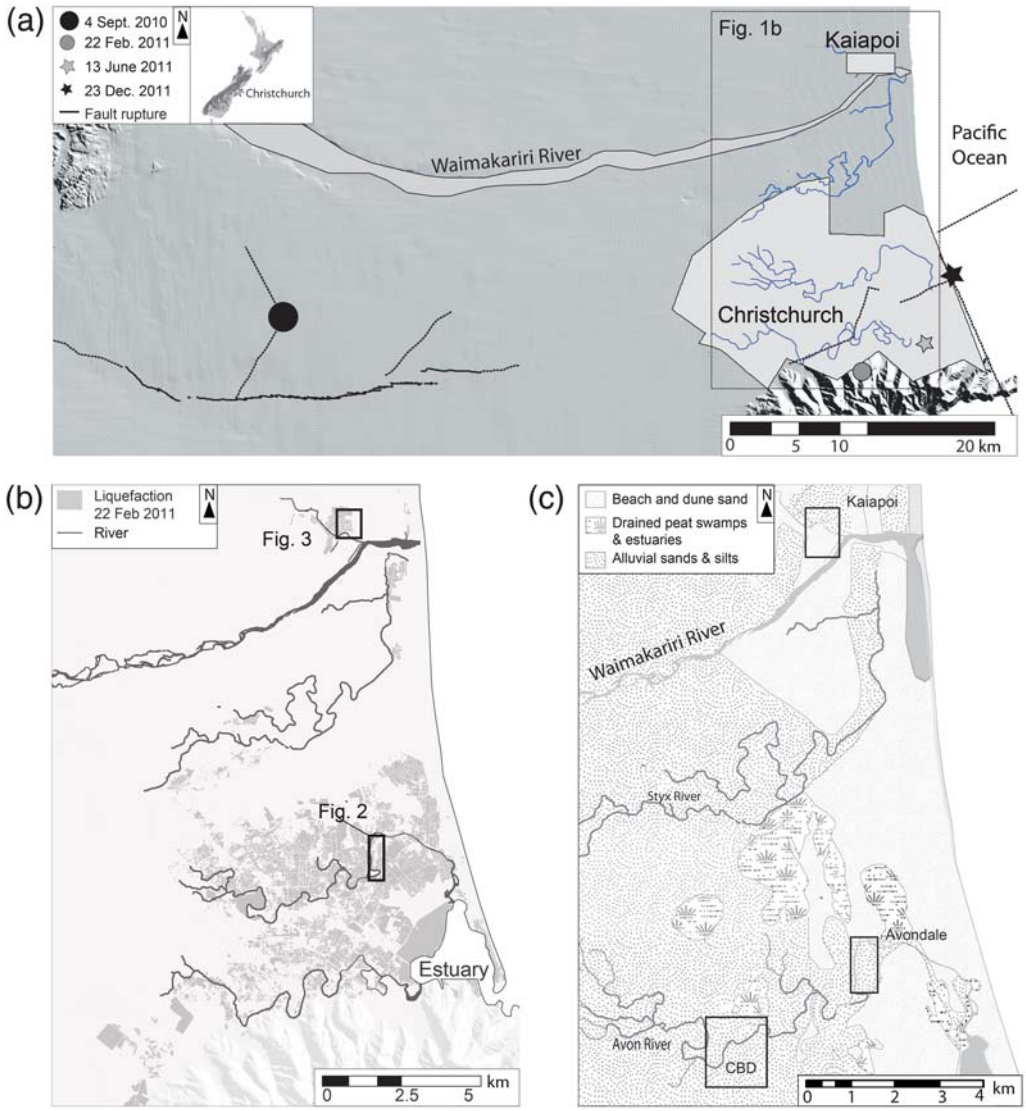

Figure 1. (a) Epicentral locations of the 2010–2011 Canterbury earthquake sequence (CES) earthquakes that triggered liquefaction within Avondale and Kaiapoi. The rupture of the Greendale fault (bold line) and projected locations of the subsurface faults that ruptured in the February, June, and December 2011 aftershocks are indicated (adapted with permission from Quigley *et al.*, 2013). (b) The aerial extent and severity of liquefaction within the wider Christchurch area as mapped following the 22 February 2011 earthquake. (c) Simplified geological map of the wider Christchurch area with locations of Avondale, Kaiapoi, and the Christchurch Central Business District (CBD) indicated.

to an anthropogenically straightened section of the meandering Avon River, which undergoes tidally influenced flow inversions. Straightening of the river was completed in 1950 to allow for improved rowing on the river. The northern extent of the suburb is encompassed by an inner depositional bank of the Avon River (Fig. 2a). The area is underlain by fine sand and silt of point bar, overbank, and adjacent swamp deposits of the Avon River (Brown and Weeber, 1992). Areas of low elevation (> 1 m.a.s.l.) adjacent to the river were in-filled by ~1 m of river dredging, comprising sand and silt, prior to the subdivision of the area in the early 1960s (Wilson, 1989). The approximate position of the ~3000 yr B.P. coastline is ~1.5 km west of the study sites; the ~2000 yr B.P. coastline was ~0.5 km to the east (Brown and Weeber, 1992). The water table is at ~1 m depth; however, this may rise to ≤0.5 m depth during wet periods (Brown and Weeber, 1992).

Three former residential properties were chosen for trenching (Fig. 2a): the site at 31 Ardrossan Street (site 1; Fig. 2b), 45 Cardrona Street (site 2; Fig. 2c), and the driveway of 53 Cardrona Street (site 3; Fig. 2d). The three sites were selected based on the intensity and alignment of liquefaction ejecta across the sites. Low elevation sites directly adjacent to the river were avoided due to the inferred presence of fill and height of the water table (~1 m).

Kaiapoi Study Area

The second study area comprises the township of Kaiapoi (population 10,200), located ~20 km north of

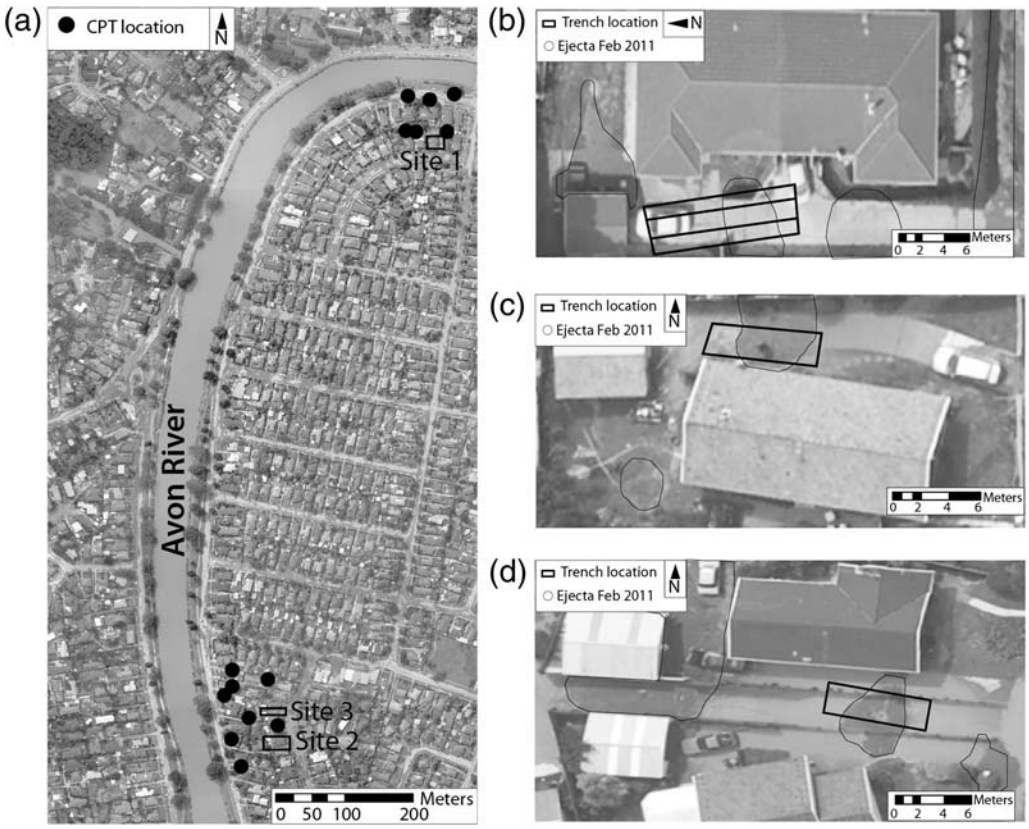

Figure 2. (a) Aerial photograph of the Avondale area with the locations of study sites 1–3 and the proximal cone penetration test (CPT) indicated. The distribution of surficial ejecta and locations of (b) T1 at site 1, (c) T2 at site 2, and (d) T3 at site 3 are also indicated.

Christchurch city and within ~4 km of the present Pegasus Bay coastline (Fig. 1). The township is situated adjacent to the banks of the Kaiapoi River on a low-relief and low-elevation alluvial landscape (0–2 m.a.s.l.). The Kaiapoi River represents the former north branch of the Waimakariri River; flow was diverted to the south branch through a canal constructed in 1868 and followed by levees in 1930 (Griffiths, 1979). The north branch became confined to a single channel within Kaiapoi, renamed the Kaiapoi River in 1969 (Wood, 1993). The area north of the Kaiapoi River is primarily underlain by fine sand of beach and dune deposits and by fine sand to silt of overbank flood deposits of the Kaiapoi River and the former north branch (Hawkins, 1957). The water table is at ~1–0.8 m depth, but this may rise to ≤0.2 m depth during wet periods (Brown and Weeber, 1992).

Two sites were chosen for trenching (Fig. 3a): the former residential property at 125 Sewell Street (site 4; Fig. 3b) and Kirk Street Reserve (site 5; Fig. 3c). Site 4 was selected because it was identified by Berrill *et al.* (1994) as likely to have liquefied during the 1901 Cheviot earthquake. Site 5 was selected because it is proximal to the area identified as liquefying during the 1901 earthquake (Berrill *et al.*, 1994), exhibited CES surface ejecta, and lacked near-surface anthropogenic influences on the spatial distribution of CES liquefaction ejecta.

Methods

Trenching

The distribution of surficial CES liquefaction features were determined at each site from high-resolution aerial photographs flown on 24 February 2011 by NZ Aerial Mapping for the Christchurch Response Centre. Trenches were excavated perpendicular to aligned sandblow vents at each site (Figs. 2 and 3). Trench walls and selected sections of the trench floor were cleaned using handheld scrapers then logged at centimeter scale to document the morphology and stratigraphic relationships of the CES and pre-CES liquefaction features. Liquefaction features and the surrounding stratigraphy were described in terms of their grain size, sorting, color, and degree of sediment mottling. Ⓔ Full sediment descriptions of each unit are presented in Table S1, available in the electronic supplement to this article. Munsell soil colors are not included in sediment descriptions because these were not obtained during trenching.

Radiocarbon Dating

Ages of the pre-CES liquefaction features and trench stratigraphy were approximated from radiocarbon dating of detrital wood and shell fragments. Dating was limited by the availability of organic material within the trenches.

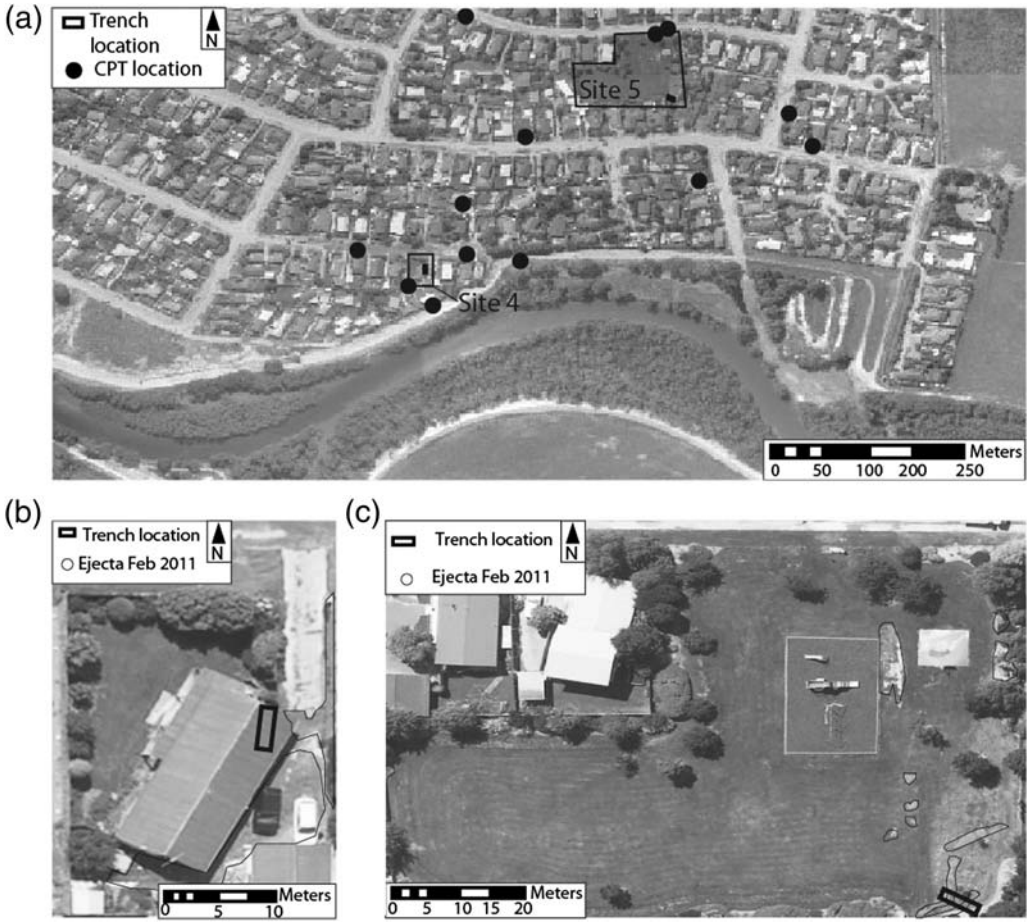

Figure 3. (a) Aerial photograph of the wider Kaiapoi area with the locations of study sites 4–5 and proximal CPT indicated. (b) Aerial photograph of site 4 following the February 2011 earthquake with the location of T4 and liquefaction ejecta indicated. (c) Aerial photograph of site 5 with the location of T5 and liquefaction ejecta indicated.

Samples of detrital wood were dried at 40°C for one week then sorted to separate the organic material from the host sediment. Between 10 and 20 mg of the organic material (charcoal or shell) was submitted to the Rafter Radiocarbon Laboratory in Wellington, New Zealand, for accelerator mass spectrometry radiocarbon analysis. Samples were prepared for analysis by subsampling, picking, and grinding of the fragments, repeated acid and alkali treatment, then combusted and converted to graphite by reduction with hydrogen over an iron catalyst. Ages were calibrated using the Southern Hemisphere calibration curve (SHCAL04; McCormac *et al.*, 2004). Radiocarbon ages are reported in the text as 2σ calendar-calibrated age ranges. Sample descriptions, uncalibrated conventional radiocarbon ages, and detailed age-range distributions of the calendar-calibrated ages are presented in Table 1.

Cone Penetration Tests

Cone penetration tests (CPTs) conducted adjacent to sites 1–5 during the CES were collated to analyze the liquefaction potential of the subsurface sediments (Figs. 2 and 3). The liquefaction potential of the subsurface sediments was evaluated using the Idriss and Boulanger (2008) method, which compares the cyclic stress ratio (CSR), that evaluates loading induced at different depths by an earthquake, with the cyclic resistance ratio (CRR), which represents the ability of the soil to resist liquefaction. The likelihood that a soil will liquefy is expressed as a factor of safety against liquefaction (FS), which is the ratio of CRR and CSR; liquefaction is predicted to trigger when FS < 1.

Study Area: Avondale

The three Avondale sites (sites 1–3; Fig. 2a) are located within 110 m of the Avon River. Site 1 is located at the apex of the meander bend and exhibits flat topography at 1.9–2 m.a.s.l. across the site (Fig. 2b). Sites 2 and 3 are located along the relatively straight section of the Avon River and exhibit elevations of 2.3–2.8 m.a.s.l. across the sites (Fig. 2). The post-February 2011 aerial photography indicates that lateral-spreading-induced fissuring and associated sandblows formed across the three sites (Fig. 2).

Trenches were excavated at each of the three sites. T1 at site 1 was excavated to a length of ~8 m and a depth of ~1.5 m, T2 at site 2 was excavated to ~5 m in length and a

Table 1
Radiocarbon Data and Age Estimates

Sample Number	Locality	Depth (m)	Trench	Description	δ13C and Source of Measurement	Radiocarbon Age (Years B.P.)	Calendar-Calibrated Age	
							2σ	1σ
R1	Avondale	1.5	Trench 1, site 1	Wood fragment from unit III	−33.6 ± −0.2	563 ± 45	A.D. 1321–1350 (10.7% of area) A.D. 1387–1453 (84.4% of area)	A.D. 1398–1439 (69.0% of area)
R2	Avondale	0.6	Trench 3, site 3	Wood fragment from unit IX	−26.6 ± 0.2	195 ± 20	A.D. 1666–1709 (25.7% of area) A.D. 1721–1812 (57.4% of area) A.D. 1837–1847 (2.4% of area) A.D. 1858–1880 (5.0% of area) A.D. 1929–1950 (4.5% of area)	A.D. 1671–1696 (21.6% of area) A.D. 1726–1747 (18.0% of area) A.D. 1756–1782 (18.5% of area) A.D. 1796–1807 (9.9% of area)
R3	Kaiapoi	0.4	Trench 4, site 4	Wood fragment from unit XIII	−27.6 ± 0.2	14,807 ± 60	16,548–16,306 B.C. (32.6% of area) 16,160–15,747 B.C. (62.5% of area)	16,496–16,376 B.C. (22.4% of area) 16,114–15,919 B.C. (45.5% of area)
R4	Kaiapoi	0.6	Trench 4, site 4	Wood fragment from unit XIII	−26.1 ± 0.2	420 ± 16	A.D. 1458–1497 (69.2% of area)	A.D. 1454–1504 (76.9% of area) A.D. 1591–1615 (18.4% of area)
R5	Kaiapoi	0.8	Trench 4, site 4	Wood fragment from unit XIII	−36.9 ± 0.2	16,452 ± 72	17,922–17,722 B.C. (32.9% of area) 17,664–17,466 B.C. (62.2% of area)	17,825–17,774 B.C. (12.9% of area) 17,631–17,491 B.C. (54.9% of area)
R6	Kaiapoi	0.3	Trench 5, site 5	Shell fragment from unit XVIII	0.7 ± 0.2	777 ± 22	A.D. 1452–1644 (95.3% of area)	A.D. 1468–1576 (67.7% of area)
R7	Kaiapoi	0.7	Trench 5, site 5	Wood fragment from unit XXII	−23.8 ± 0.2	703 ± 16	A.D. 1297–1314 (29.7% of area) A.D. 1359–1381 A.D. (39.8% of area)	

depth of ~0.9 m, and T3 at site 3 was excavated to a length of ~3 m and depth of ~1.1 m (Fig. 2). Trench depths were limited by the depths to the water table, which was at ≤1.5 m during excavation.

Trench Stratigraphy

T1, shown in Figure 4a, exposed stratigraphy comprising a basal nonplastic silt to very fine sand (unit II) with an interbedded lens of fine to very fine sand (unit III) and overlain by carbonaceous silt to very fine sand (unit I). The stratigraphy is capped by silt to fine sand with granules (unit A3), silt to very fine sand (unit A2), and granules (unit A1; Fig. 4a).

T2, shown in Figure 4b and c, exposed a basal nonplastic silt with interbedded very fine sand (unit VI), which is overlain by carbonaceous, very fine sand to silt (unit IV) that contains a lens of fine to very fine sand (unit V). The stratigraphy is capped by granules (unit Al; Fig. 4b,c).

T3, shown in Figure 4d, exposed a basal fine to very fine sand (unit X; Fig. 4d) with an interbedded lens of carbonaceous very fine sand to silt (unit XI). This is overlain by carbonaceous very fine sand (unit VIII) with interbedded lenses of fine to very fine sand (unit IX) and capped by carbonaceous, very fine sand to silt (unit VII). Ⓔ Full sedimentological descriptions of each unit are presented in Table S1.

The stratigraphy exposed in the three trenches (T1–T3) is mottled and oxidized below ~0.5 m depth. The nonplastic silts to very fine sands exposed in T1–T3 (units II, IV, VI, and XI) are interpreted as low-energy overbank flood deposits of the Avon River (Fig. 4). The fine to very fine sands (units III, V, VIII, IX, and X) suggest that the floodplain periodically received sediment during flood events (Fig. 4). The fluvial stratigraphy is consistent with the inferred pre-European migration of the Avon River across the site and with historical reports of periodic flooding of the Avon River during periods of heavy rain between 1865 and 1953 (Cowie, 1957).

Unit IV in T2 and unit VII in T3 (Fig. 4a–d) are interpreted as topsoil horizons. There are no well-documented rates of soil formation for the Canterbury urban area due to the varied land uses throughout the development of the region, thus no surface age may be inferred from soil thickness. Unit I, exposed in T1 (Fig. 4a), is interpreted as a buried soil horizon based on the similar appearance to units IV and VII and the

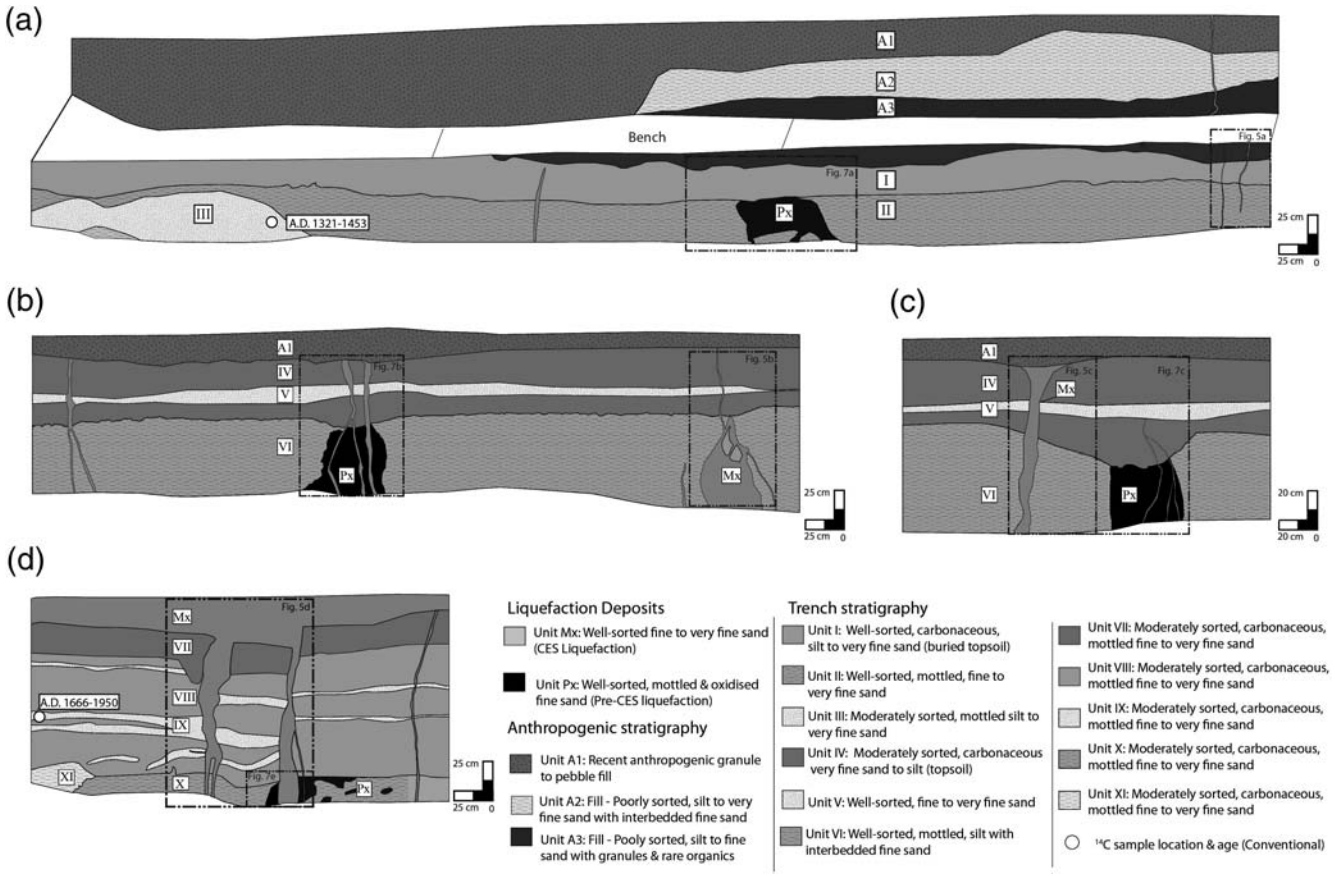

Figure 4. (a) Detailed log of the west wall of T1 excavated at site 1 in Avondale. The CES liquefaction dikes (Mx 1–Mx 3) crosscut the fluvial (I–II) and anthropogenic stratigraphy (A1–A3). The pre-CES dike (Px 1) crosscuts the fluvial stratigraphy (II) and is overlain by the buried topsoil (I). The location and result of the ^{14}C sample R1 is also indicated. (b) Detailed log of the north wall of T2 at site 2 in Avondale. The CES dikes (Mx 1–Mx 5) crosscut the fluvial stratigraphy (IV–VI) and are truncated by the post-CES anthropogenic fill (A1). The pre-CES dike (Px 2) crosscuts the fluvial stratigraphy (VI) and is truncated by unit IV, which thickens in the area directly overlying the dike. (c) Detailed log of the south wall of T2 at site 2. The pre-CES dike (Px 2) can be traced across the trench floor and up the south wall, where it also crosscuts the fluvial stratigraphy to beneath unit IV. (d) Detailed log of the north wall of T3 excavated at site 3. The CES dikes (Mx 1–Mx 3) crosscut the fluvial stratigraphy (IV–I) and dissipate into the surface ejecta (Mx). A bulbous feature, possibly comprising a pre-CES injection feature (Px 3), crosscuts unit X and is crosscut by unit VIII. The location and result of the ^{14}C sample R2 is also indicated. Locations for the detailed images shown in Figures 5 and 7 are included (dotted–dashed rectangles).

presence of modern rootlets. It is likely that unit I is associated with the infilling of the area prior to its subdivision (Wilson, 1989). Unit A3, which overlies unit I, is interpreted as the river dredging used to infill the site and mixed with granules that were likely deposited during construction at the site (Fig. 4a). Unit A2 was likely deposited during occupation at the site post-1860. The surficial granules exposed in T1 and T2 (unit A1; Fig. 4) are interpreted as post-CES deposits associated with the demolition of the former residential dwellings, subsequent waste removal, and leveling of the site.

Radiocarbon dating of two samples of subrounded wood fragments, sample R1 obtained from unit III at 1.5 m depth in T1 (Fig. 4a) and sample R2 from unit IX in T3 at 0.6 m depth (Fig. 4d), yielded ages of A.D. 1321–1453 and A.D. 1666–1950, respectively (Table 1). Both R1 and R2 lacked root-like geometries, suggesting that they were of detrital origin, thus the reported ages are interpreted to approximate the maximum depositional ages of the sediment.

CES Liquefaction Features

CES liquefaction features were recognized in the subsurface by (1) their alignment with and traceable continuity into the observed surface CES features and (2) their crosscutting relationships with the trench fluvial stratigraphy. The morphologies of the subsurface CES liquefaction features are documented in detail to assist with the identification and interpretation of pre-CES liquefaction features.

The surface sandblows intersected in T1–T3 correspond with subvertical and planar dikes in the subsurface (Fig. 4). The dikes vary in width from 1 to 3 cm in T1, 3 to 9 cm in T2, and 2 to 15 cm in T3. The $<$2-cm-wide dikes in T1 (Figs. 4a and 5a) are composed of well-sorted silt to very fine sand, whereas the $<$2-cm-wide dikes in T1–T3 are all coarser and composed of well-sorted fine to very fine sand (unit Mx). The dikes all increase in width with depth and lack the oxidation and mottling developed in the surrounding stratigraphy

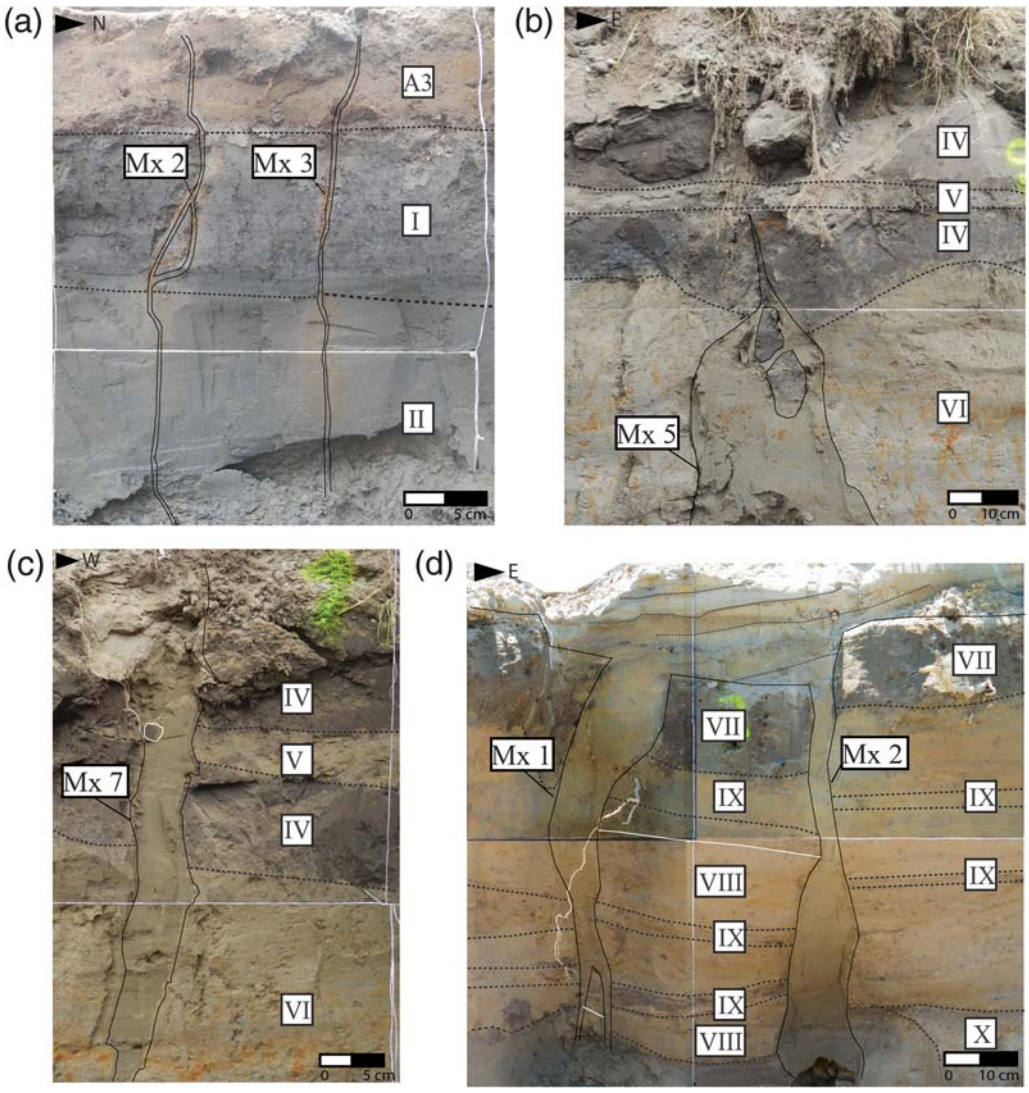

Figure 5. (a) Interpreted field photograph of the west wall of T1 (site 1; Avondale). The CES liquefaction dikes (Mx 2–Mx 3; outlined in black solid line) crosscut the fluvial (I–II) and anthropogenic stratigraphy (A3; outlined in black dotted lines). (b) The fluvial stratigraphy (IV–VI) on the north wall of T2 (site 2; Avondale) is crosscut by a CES injection feature that feeds into a CES dike (Mx 5; outlined in black). (c) The fluvial stratigraphy (unit IV–VI; outlined in black dotted line) on the south wall of T2 (site 2; Avondale) is crosscut by a CES subvertical and planar liquefaction dike (Mx 7; outlined in black). (d) The fluvial stratigraphy (VII–X) on the north wall of T3 (site 3; Avondale) is crosscut by two subvertical and planar CES dikes (Mx 1–Mx 2) that feed into the CES surface ejecta (Mx). Silt drapes preserved within the surface ejecta (black dashed lines) indicate multiple events are preserved within the ejecta.

(Figs. 4 and 5). Dikes in T1 and T2 crosscut the fluvial stratigraphy from the trench floor and are truncated by the post-CES fill (unit A1), thus indicating that they formed during the CES (Figs. 4 and 5). The dikes in T3 crosscut the stratigraphy from the trench floor to the surface, where they dissipate into the surficial fine to very fine sand with internal silt drapes (Mx). The surficial sediment is of consistent texture to the liquefaction ejecta within the dike and corresponds with the location of surface ejecta observed in Figure 2 and is therefore interpreted as liquefaction ejecta. The internal silt drapes within the liquefaction ejecta are consistent with the silt drapes that separate multiple episodes of liquefaction within a compound sand blow described by Quigley *et al.* (2013). The ejecta is therefore interpreted as preserving evidence for 5 episodes of liquefaction.

Dikes that crosscut the fluvial stratigraphy from the trench floor to between 0.5 and 0.7 m depth, where they pinch out and terminate, were also observed in T1 (Mx 1 and Mx 3; Figs. 4 and 5) and T2 (Mx 4 and Mx 7). The similar morphologies, textures, and lack of oxidation and mottling in these dikes indicate that they are also of CES age (Figs. 4 and 5). A dike (Mx 5) on the north wall of T2 extends upward from a bulbous-shaped feature that exhibits sharp contacts with the surrounding fluvial sediment and is composed of fine sand with silt clasts (Figs. 4b and 5b). The morphology of this feature, combined with its lack of mottling and oxidation, indicates that it comprises a CES subsurface injection feature (Figs. 4b and 5b).

The increasing width of the dikes with depth supports that these dikes formed by the upward injection of liquefied sedi-

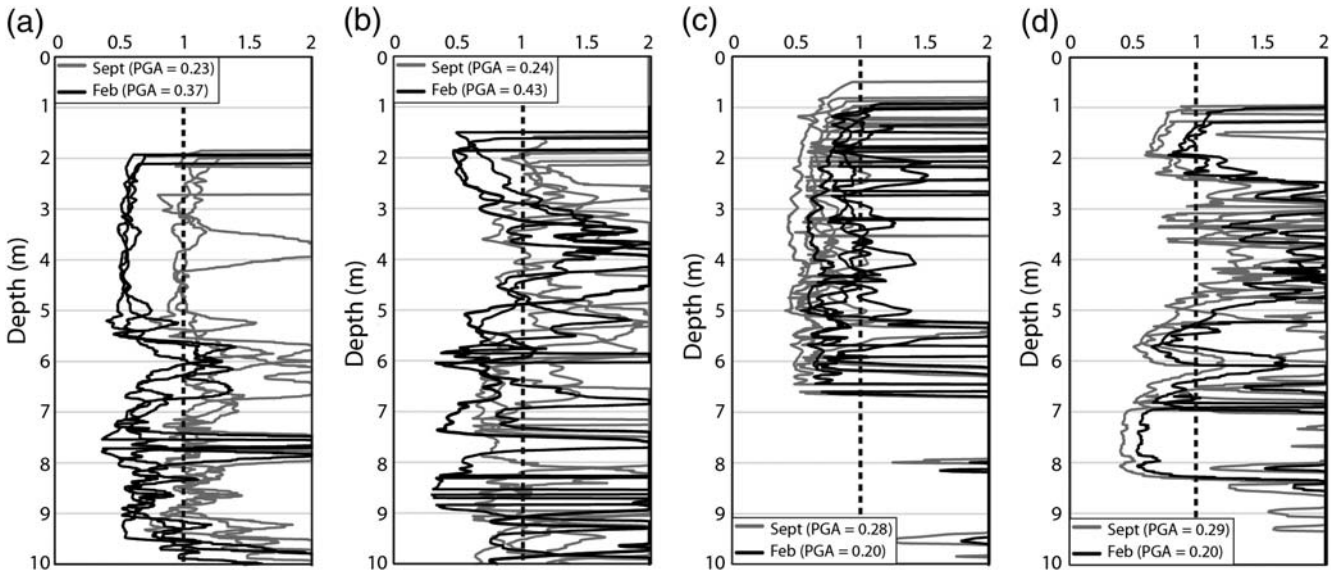

Figure 6. (a) The CPT conducted proximal to site 1 indicate that the sediment from 2.6 to 5 m depth and beneath 7.5 m likely liquefied (FS < 1) under the peak ground acceleration (PGA) generated in the September 2010 earthquake, whereas the sediment beneath 2 m depth likely liquefied (FS < 1) in the February 2011 earthquake. (b) At sites 2 and 3, the sediment profile beneath 2.2 m likely liquefied (FS < 1) under the PGA of the September earthquake, whereas the sediment from 1.8 to 3.2 m and beneath 5 m depth likely liquefied (FS < 1) during the February 2011 earthquake. (c) At site 5, the CPT indicate that the sediment beneath 0.5 m likely liquefied (FS < 1) during the September 2010 earthquake, whereas beneath 1.1 m depth likely liquefied during the February 2011 earthquake. (d) At site 6, the sediment profile beneath 1.0 m depth contains layers that likely liquefied during the September earthquake, whereas the sediment beneath 1.2 m depth contains thin layers that likely liquefied during the February 2011 earthquake.

ment, as opposed to surface cracking in which features typically decrease in width with depth (Figs. 4 and 5; Counts and Obermeier, 2012). The varied widths of the dikes identified in T1–T3 may reflect variations in the 3D geometries of the dikes. The subvertical planar morphology and well-sorted grain-size distributions of these CES dikes and injection feature are consistent with the morphology and texture of dikes previously described in detail in Counts and Obermeier (2012) and Bastin *et al.* (2015). The consistent morphologies of the liquefaction features indicate that liquefaction is likely to manifest in the geologic record as subvertical planar dikes that increase in width with depth, are composed of well-sorted sediment, and are of varying widths.

The CPT soundings conducted proximal to site 1 indicate that the sediment profile from 2.6 to 5 m depth and beneath 7.5 m at site 1 likely liquefied (FS < 1) during the September 2010 earthquake, whereas the sediment beneath 2 m depth likely liquefied (FS < 1) during the February 2011 earthquake (Fig. 6). At sites 2 and 3 the subsurface sediment contains thin layers beneath 2.2 m depth that were potentially liquefiable (FS < 1) during the September 2010 earthquake (Fig. 6). The sediment from 1.8 to 3.2 m depth and beneath 5 m depth likely liquefied (FS < 1) during the February 2011 earthquake. The exact source depth of the liquefied sediment cannot be determined directly, because excavation was limited by the depth to the water table. The predominately gray, well-sorted, silt to fine sand texture of the CES dikes identified in T1–T3 suggests that a liquefiable unit or units containing fine sand to silt exists at depth beneath the three sites.

Pre-CES Liquefaction Features

Pre-CES liquefaction features were identified in T1-T3 based on their mottling and oxidation, morphology, and crosscutting relationships with the CES liquefaction features and surrounding stratigraphy.

Subvertical and planar dikes ~20–40 cm wide and composed of mottled and oxidized well-sorted fine sand to silt (unit Px) crosscut unit II in T1 (site 1) and unit VI in T2 (site 2; Figs. 4 and 7). The subvertical and planar morphology and the well-sorted texture of these dikes are consistent with the CES dikes identified within T1–T3. At site 1, the dike (Px 1) is truncated by unit I and exhibits no evidence for surface ejecta. It could not be determined whether the dike continued across the trench floor due to flooding of the trench; however, the dike was not observed on the opposite trench wall. At site 2, the oxidized dike (Px 2) in T2 is overlain by unit IV, which thickens from ~35 to ~60 cm in the area above Px 2 (Figs. 4b,c and 7b). The dike (Px 2) could be traced across the trench floor, where it corresponds with a dike (Px 2) on the south wall that is also overlain by unit IV (Fig. 7c,d). In T3, a CES dike (Mx 2) crosscuts an irregular, bulbous-shaped feature that is ~10 cm wide and composed of mottled and oxidized fine sand to silt with silt clasts (Px 3). Px 3 crosscuts unit X and is crosscut by unit VII (Figs. 4d and 7e). It could not be determined whether the feature (Px 3) was dike fed because excavation was limited by the depth to the water table. The feature could not be traced across the trench floor due to flooding and could not be identified on the opposite trench wall.

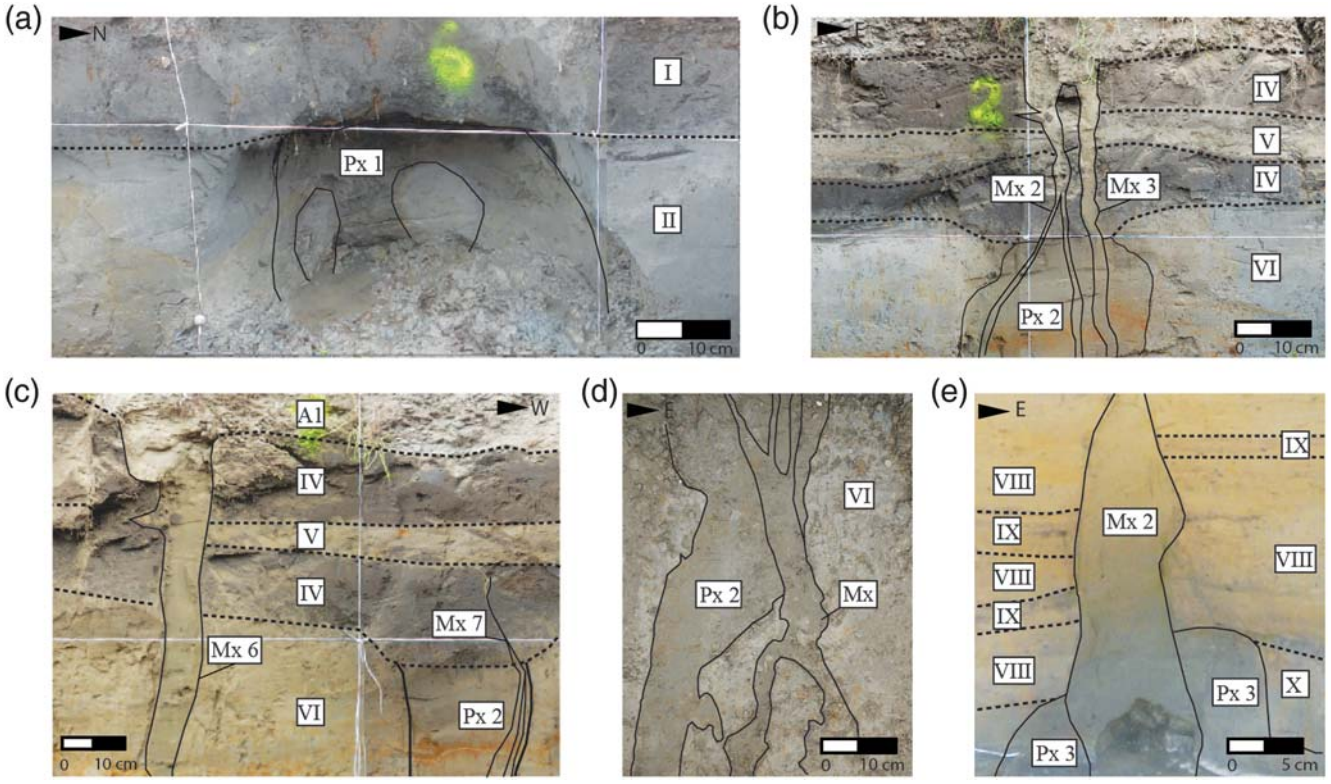

Figure 7. (a) Interpreted field photograph of the west wall of T1 (site 1; Avondale). The pre-CES dike (Px 1; outlined in black) crosscuts the fluvial stratigraphy (unit IV; outlined in black dotted line) and is truncated by the buried soil (unit I). (b) Interpreted field photograph of the north wall of T2 (site 2; Avondale) indicating the alignment of the CES (Mx 2–Mx 3; outlined in black) and pre-CES dikes (Px 2). Px 2 crosscuts unit VI and is overlain by unit IV, which thickens in the area overlying Px 2. (c) Interpreted field photograph of the south wall of T2 (site 2). (d) The CES dike (Mx) also crosscuts the pre-CES dike (Px 2) on the trench floor. (e) Interpreted field photograph of the north wall of T3 (site 3; Avondale). The CES dike (Mx 2; outlined in black) crosscuts the fluvial stratigraphy and the bulbous feature that possibly comprises a pre-CES injection feature (Px 3).

The subvertical and planar morphology of the oxidized and mottled dikes exposed in T1 (site 1) and T2 (site 2) suggest that they comprise pre-CES dikes or lateral-spreading fissures (Fig. 4a). The lateral traceability and morphology of Px 2 in T2, combined with the thickening of unit IV in the area overlying the dike, suggests that the feature comprises a lateral-spreading fissure that was infilled by flood deposits while exposed at the surface (Figs. 4b and 7b,c,d). The sharp contacts and morphology of Px 3 in T3 are similar to the bulbous CES feature (Mx 5) identified in T2, suggesting that Px 3 may have formed through the subsurface injection of liquefied sediment (Fig. 4d). This cannot be confirmed, because no dike feeding the feature was observed. However, the silt clasts within Px 3 are consistent with inclusions observed within the CES features and attributed to the fragmentation and entrainment of host sediment during ejection of liquefied sediment (Bastin *et al.*, 2015). This supports the interpretation that Px 3 comprises a pre-CES injection feature.

The mottling and oxidation of the sediment within Px 1–3 forms through the precipitation of reduced iron in pore spaces during lowering of the water table (van Breemen and Buurman, 2002). The presence of well-developed mottles and oxidation in Px 1–Px 3 suggests long residence within fluctuating water tables and thus indicates pre-CES emplacement. To the best of our knowledge, no empirical data constraining the rate of mottle formation in a subsurface deposit under fluctuating water tables have been established for the Canterbury region, thus no absolute age for dike emplacement can be determined from the degree of sediment mottling.

Px 1 in T1 crosscuts unit II, indicating that it postdates deposition of this unit, dated at A.D. 1321–1453 by radiocarbon (sample R1; Fig. 4a). No evidence for surface ejecta or a buried surface was observed, suggesting that the top contact was likely truncated prior to or during deposition and formation of the buried soil (unit I). Px 2 in T2 crosscuts unit VI and is overlain by unit IV (Fig. 4b). No samples suitable for dating were identified in T2; however, it may be inferred that the maximum depositional age of A.D. 1321–1453 derived for unit II in T1 from radiocarbon approximate the depositional age of unit VI in T2 based on the proximity of the sites and similar stratigraphies. Px 2 may therefore postdate the radiocarbon age. Px 3 in T3 is crosscut by unit VIII, indicating that injection may predate the radiocarbon age of A.D. 1666–1950 derived for unit IX interpreted as a maximum depositional age (Table 1; Fig. 4c).

The CES and pre-CES features identified in T1–T3 are all composed of well-sorted silt to fine sand, which indicates that there are liquefiable units at depth containing fine sand

to silt. The liquefiable source unit(s) was not observed within these trenches, and it therefore could not be determined whether the CES and pre-CES features were sourced from the same unit at depth.

Study Area: Kaiapoi

The two Kaiapoi sites (sites 4–5; Fig. 3a) are located adjacent to an outer meander bend of the Kaiapoi River. The post-February 2011 aerial photography indicates that localized and aligned sandblows formed across both sites (Fig. 3). Trenching revealed stratigraphy that could not be correlated between the two sites, thus the two sites are discussed separately.

Site 4: Sewell Street

Site 4 is located within 75 m of the Kaiapoi River at 125 Sewell Street (Fig. 3b). The site exhibits relatively flat topography at 2.4–2.6 m.a.s.l. A trench (T4) was excavated to a length of ~2.5 m and a depth of ~0.9 m following the demolition of the former residential dwelling (Fig. 3b). The depth of the trench was limited by the depth to the water table, which was at ≤0.9 m during excavation.

Trench Stratigraphy. The trench exposed stratigraphy comprising a basal silt to very fine sand (unit XIII) with interbedded lenses of silt to very fine sand with cross laminations (unit XIV), fine to very fine sand (unit XV), and fine to very fine sand with silt laminations (unit XVI; Fig. 8). Unit XIII is overlain by silt to very fine sand on the northern wall (unit XII; Fig. 8) and granules on the eastern wall (unit A1; Fig. 8). The stratigraphy is mottled from ~0.3 m depth. Ⓔ Full sedimentological descriptions of each unit are presented in Table S1.

Unit XIII is interpreted as a low-energy floodplain deposit, whereas the interbedded silts with cross laminations and fine to very fine sands (units XIV, XV, XVI) indicate that the site was periodically flooded (Fig. 8). The fluvial stratigraphy is consistent with the present depositional setting within the low elevation (~2 m.a.s.l.) floodplain of the Kaiapoi River and historical reports of flooding of the Kaiapoi River and former north branch of the Waimakariri River (Hawkins, 1957; Logan, 2008). The poorly sorted granules on the east wall (unit A1; Fig. 8a) are interpreted as post-CES fill. Unit XII on the north wall is interpreted as a topsoil horizon (Fig. 8).

Radiocarbon dating of three detrital wood fragments obtained from unit XIII at depths of 0.4 m (sample R3), 0.6 m (sample R4), and 0.8 m (sample R5) yielded ages of 16,548–15,747 B.C. (sample R3), A.D. 1458–1497 (sample R4), and 17,922–17,466 B.C. (sample R5), respectively (Table 1; Fig. 8). Samples R3 and R5 provided age spectra inconsistent with sample R4 and the geologic evolution of the Canterbury coastline, indicating that they likely comprised older, reworked detritus (Brown and Weeber, 1992; Forsyth *et al.*, 2008). Samples R3 and R5 are therefore excluded from further discussions. Sample R4 was composed of a small, subrounded wood fragment that lacked root-like geometries or lateral continuity, thus suggesting that it was of detrital origin. The A.D. 1458–1497 age range of sample R4 is consistent with the geologic evolution of the Canterbury coastline (Brown and Weeber, 1992). The age is therefore interpreted as the maximum depositional age of unit XIII, with the actual depositional age possibly much younger.

CES Liquefaction Features. The CES features were documented in detail to determine whether the morphologies of liquefaction features are consistent in the fluvial deposits of both the Avon and Kaiapoi Rivers and to aid identification of pre-CES features. The CES features are all composed of well-sorted fine to very fine sand and lack the oxidation and mottling developed in the surrounding stratigraphy (unit Mx; Fig. 8).

T4 exposed three subvertical and planar dikes in the subsurface (Mx 1–Mx 3). Dike Mx 1 crosscuts the stratigraphy from the trench floor to ~0.5 m depth, where it pinches out and branches into an ~20–30-cm-long, laterally injected sill (Figs. 8a and 9b). Dikes Mx 2 and Mx 3 vary in width from ~2 to 5 cm and exhibit a complex branching pattern (Figs. 8 and 9a). Dikes Mx 2–3 crosscut the fluvial stratigraphy and are truncated by unit A1, indicating that they predate deposition of unit A1 (Fig. 8). The lack of oxidation and mottling within Mx 1–Mx 3 indicates their recent emplacement and thus suggests that they formed during the CES. The dikes all increase in width with depth and contain no evidence for vertical and/or lateral grading.

The CPT soundings indicate that the sediment profile beneath 0.5 m depth likely liquefied (FS < 1) during the September 2010 earthquake, whereas the sediment beneath 1.1 m depth likely liquefied (FS < 1) during the February 2011 earthquake (Fig. 6c). The exact source depth for the dikes cannot be determined directly because excavation was limited by the depth to the water table.

Pre-CES Liquefaction Features. The CES dike (Mx 3) on the east wall of T4 crosscuts an irregular sill with bioturbated contacts and comprised of well-sorted, oxidized, and mottled fine to very fine sand with internal silt drapes and silt clasts (Px 4; Figs. 8a and 9a). Px 4 crosscuts unit XIII from ~60–65 cm depth; it exhibits a morphology consistent with the adjacent CES sill and a texture consistent with the pre-CES dikes identified in T1 and T2.

Unit XIII on the north wall is interbedded with a mound-shaped feature at ~85–95 cm depth that is composed of well-sorted, oxidized, and mottled fine sand (Px 5; Figs. 8b and 9b,c). The feature (Px 5) contains a silt-lined basal contact and two internal horizontal silt drapes, and it decreases in thickness toward the eastern and western walls of the trench (Figs. 8b and 9c,d). An ~2-cm-wide subvertical and planar dike extends from the trench floor and into the base of Px 5 at its thickest point. The dike exhibits a grain-size distribution and texture consistent with the feature and can be traced through

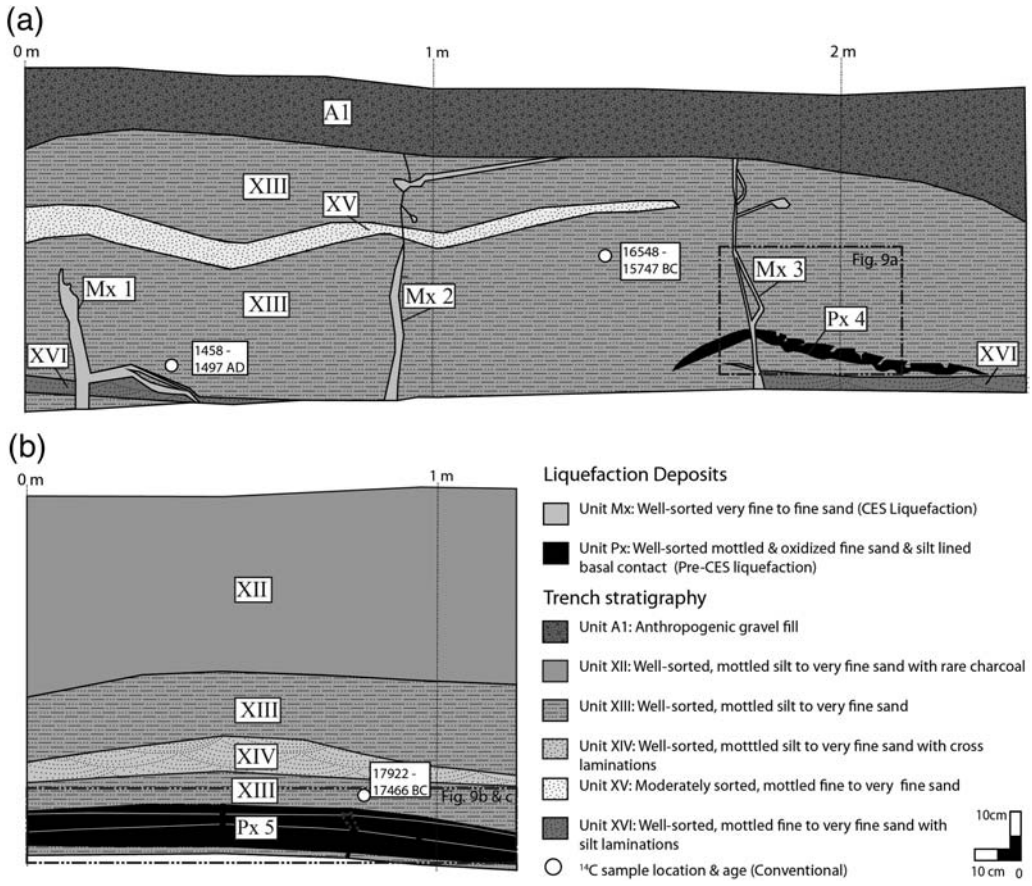

Figure 8. (a) Detailed trench log of the east wall of T4 (site 4; Kaiapoi). The CES liquefaction dikes (Mx 1–Mx 3) crosscut the fluvial stratigraphy. Mx 3 1 crosscuts the stratigraphy to ~40 cm depth, where it pinches out, whereas Mx 2–Mx 3 are truncated by the post-CES anthropogenic fill (A1). Dike Mx 3 crosscuts an irregular sill with bioturbated contacts and is interpreted as a pre-CES sill (Px 4). (b) On the north wall of T4 (site 4; Kaiapoi), a dike-fed pre-CES sandblow (Px 5) that contains two internal silt drapes is buried at ~95 cm depth within the fluvial stratigraphy. The locations and results of the ^{14}C samples are also indicated. Locations of the photographs in Figure 9 are indicated by the dotted–dashed rectangles.

the feature, where it crosscuts the internal silt drapes and appears to dissipate into the upper unit of fine sand (Fig. 9b,c).

The mottling and oxidation formed within the sill (Px 4) and mound-shaped feature (Px 5) indicates their prolonged residence within fluctuating water tables and thus indicates pre-CES emplacement (Figs. 8 and 9). The morphology, texture, and presence of silt clasts within Px 4 indicate that it comprises a pre-CES laterally injected sill, whereas its bioturbated contacts suggest emplacement occurred very near the surface. No dike feeding the sill was observed; however, it is possible that it was reactivated by the CES dike or that the dike was not intersected within the trench. The sill crosscuts unit XIII, indicating that injection postdates the maximum depositional age of this unit dated at A.D. 1458–1497 by radiocarbon (sample R4; Table 1).

The dike beneath the oxidized mound-shaped feature (Px 5) indicates that it formed by the upward ejection of liquefied sediment (Figs. 8b and 9c). The morphology and texture of Px 5 is consistent with a CES compound sandblow observed at another site by Quigley *et al.* (2013) that contained four episodes of liquefaction composed of oxidized fine sand grading to gray fine sand and overlain by a silt drape that could not be traced through the vent zone (Fig. 9). Px 5 is therefore interpreted as a pre-CES sandblow, while the presence of two internal silt drapes suggests that three distinct episodes of liquefaction are preserved within the sandblow (Fig. 9b). No upper silt-lined contact was observed, indicating that the upper surface was likely reworked. This should therefore be treated as the minimum number of liquefaction events. The pre-CES compound sandblow would have formed at the ground surface at the time of the pre-CES earthquake, indicating that ~0.95 m of sedimentation has since occurred at the site. The higher stratigraphic position of Px 4 in T4 (~60–65 cm depth) indicates that two separate events are preserved within the stratigraphy.

Site 5: Kirk Street Reserve

Site 5 is located within 200 m of the Kaiapoi River and comprises relatively flat topography at 2.3–2.8 m.a.s.l. across the site. A trench (T5) was excavated to a length of ~6 m and a depth of ~1.2 m (Fig. 3c). The depth of the trench was

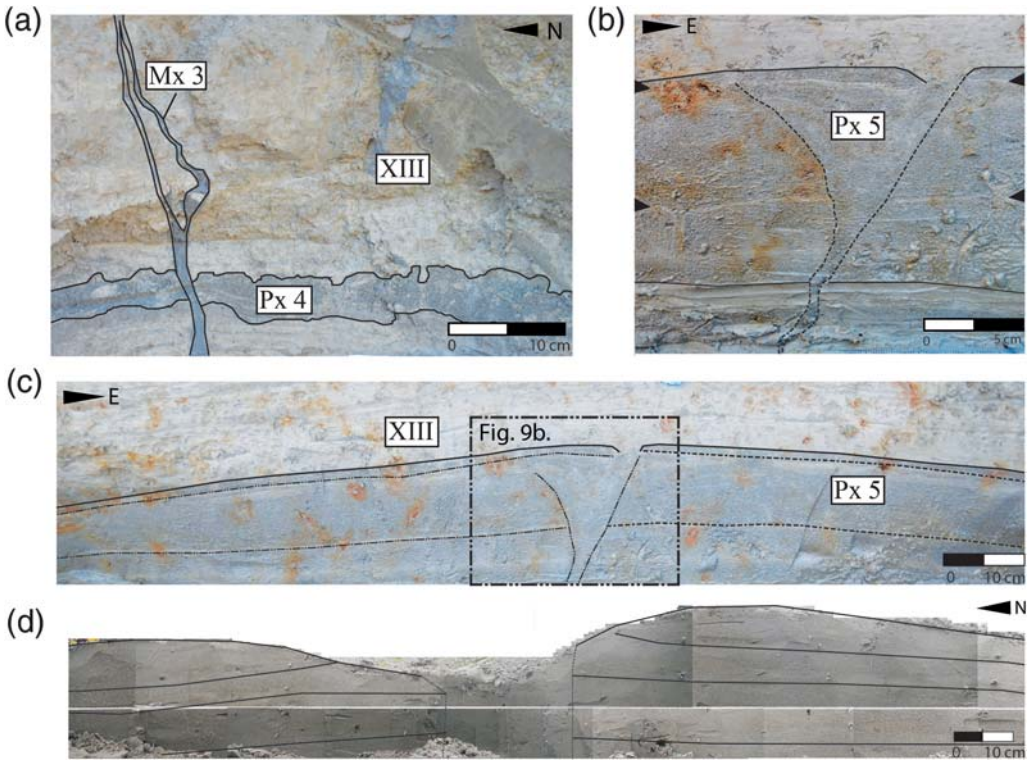

Figure 9. (a) Interpreted field photograph of the east wall of T4 (site 4; Kaiapoi). The CES dike (Mx 3) crosscuts the fluvial stratigraphy (unit XIII) and the pre-CES lateral sill (Px 4), which exhibits bioturbated contacts. (b,c) Close-up interpreted field photographs of the north wall of T4 (site 4). The fluvial stratigraphy (unit XIII) contains a dike-fed pre-CES sandblow (Px and outlined in black) that contains two internal silt drapes (arrows in b and dashed black lines in c) that cannot be traced through the vent zone. The location of Figure 9b is outlined in a dotted–dashed rectangle in (c). (d) Interpreted field photograph of a CES sandblow (outlined in black), which contains internal silt drapes (black dashed lines) that cannot be traced across the vent zone (adapted with permission from Quigley *et al.*, 2013).

limited by the depth to the water table, which was at ~1.3 m during excavation.

Trench Stratigraphy. The north wall of the trench exposed stratigraphy comprising a basal silt to very fine sand (unit XXIV; Fig. 10a) overlain by fine to very fine sand with granules and silt clasts (unit XXIII). Unit XXIII contains irregular and deformed lenses composed of fine to very fine sand with rare granules and carbonaceous silt clasts (unit XX), fine sand with cross laminations and rare silt clasts (unit XXI), and a clast of unit XXIV. The lenses of unit XX and XXI warp around fragmented clasts comprised of silt to very fine sand with rare granules (unit XXII; Fig. 10a and 11a). The lenses of units XX and XXI all appear deformed, are poorly sorted, and exhibit no evidence for vertical grading or internal structure. Unit XXIII is overlain by normally graded, fine to very fine sand with granules and silt clasts interbedded with fine sand with cross laminations (unit XVIII) and silt with rare granules and silt clasts (unit XVII).

The south wall exhibits similar stratigraphy of unit XXIV overlain by unit XXIII and lenses of unit XXI, which contains fragments of XXII. These are overlain by unit XIX, which is composed of normally graded, fine to very fine sand with cross laminations, and a granule-lined basal contact (Fig. 10b). The stratigraphy is capped by unit XVIII and a granule-to-pebble-rich horizon (unit XVIII′) that are crosscut by unit XVII (Fig. 10b). The stratigraphy is mottled from ~60 cm depth. Ⓔ Full sedimentological descriptions of each unit are presented in Table S1.

Unit XXIV is interpreted as a low-energy overbank deposit of the Kaiapoi River or former north branch of the Waimakariri River (Fig. 10). The normally graded sands (units XIX and XVIII) and the granule horizon (XVIII′) on the south wall are interpreted as overbank flood deposits. Unit XVII is interpreted as a topsoil horizon (Fig. 10). The deformation within unit XXIII and lenses of units XX and XXI are inconsistent with the inferred fluvial floodplain deposition of the stratigraphy due to their poorly sorted grain-size distributions and irregular and deformed morphologies (Figs. 10a and 11a). It is possible that units XX and XXI comprised normally graded fluvial deposits, similar to unit XIX, prior to their deformation. The fragments of XXII exhibit a morphology inconsistent with the surrounding lenses and a composition that is similar to unit XVII. Unit XXII is therefore interpreted as a fragmented buried soil horizon.

Radiocarbon dating of a shell obtained from unit XVIII at 0.3 m depth (sample R6) yielded an age of A.D. 1452–1644, whereas a wood fragment obtained from unit XXIII at 0.7 m depth (sample R7) yielded a radiocarbon age of A.D. 1297–1381 (Table 1). The reported radiocarbon age

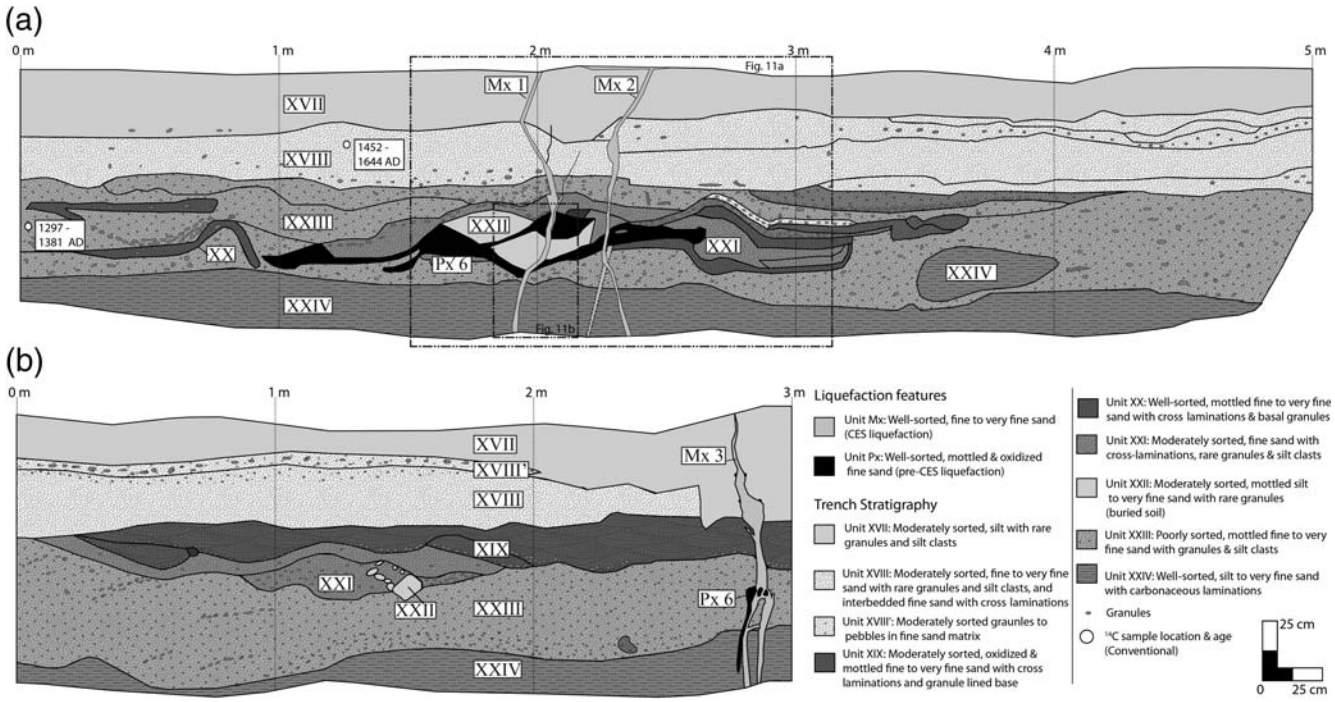

Figure 10. Detailed trench log of the (a) north and (b) south walls of T5 (site 5; Kaiapoi). The CES dikes (Mx 1–Mx 3) crosscut the stratigraphy from the trench floor to the surface. (a) Unit XXIII on the north wall contains a fragmented buried topsoil (unit XXII) and lenses that exhibit soft sediment deformation (XX–XXI). The deformed stratigraphy is interfingered with a pre-CES liquefaction feature (Px 6) interpreted as comprising a buried pre-CES sandblister. The locations and results of the ^{14}C samples are indicated. The location of the photographs in Figure 11 is indicated by the dotted–dashed rectangle.

of the shell (sample R6) is inconsistent with the timing of the historical shorelines that are well documented through the area, thus suggesting that it may have been deposited by anthropogenic activity (Brown and Weeber, 1992). Sample R7 was composed of a small, subrounded wood fragment that lacked root-like geometries or lateral continuity, suggesting that it comprised detritus; it is therefore interpreted to reflect the maximum depositional age of the sediment.

CES Liquefaction Features. The surface sandblows correspond with 2–4-cm-wide subvertical and planar dikes in the subsurface (Mx 1–3; Fig. 10). The dikes crosscut the stratigraphy from the trench floor to the surface, indicating that they were emplaced during the CES (Figs. 10 and 11). The margins of Mx 1–Mx 3 are surrounded by an oxidized lining and pockets of oxidized fine sand from the trench floor to ~75 cm depth. The oxidation suggests that the lining and pockets of fine sand predate the CES (Figs. 10 and 11b). Above 75 cm depth, the dikes lack the oxidation and mottling developed in the surrounding stratigraphy (Figs. 10 and 11a,b). The dikes are all composed of well-sorted fine to very fine sand, increase in width with depth, and contain no evidence for vertical grading.

The CPT soundings conducted adjacent to site 5 indicate that the sediment profile beneath 1.1 m depth contains layers that likely liquefied (FS < 1) during the September 2010 earthquake, whereas the sediment beneath 1.2 m depth contains layers that likely liquefied (FS < 1) during the February 2011 earthquake (Fig. 6d). The exact source depth cannot be determined directly because excavation to this depth was limited by the depth to the water table.

Pre-CES Liquefaction Features. A pre-CES liquefaction feature was identified in T5 based on its oxidation and mottling, well-sorted grain-size distribution, and its crosscutting relationships with the CES features and surrounding stratigraphy.

The irregular and deformed lenses of units XX and XXI within unit XXIII are interfingered with an irregular and complex branching feature (Px 6) composed of oxidized and mottled well-sorted fine sand (unit Px; Figs. 10a and 11a). The feature (Px 6) interfingers with the deformed units XX and XXI from ~75 to 60 cm depth and appears to intrude around the contacts of the fragmented topsoil (unit XXII; Fig. 10a). The feature could not be identified on the south wall. The deformation and poorly sorted grain-size distributions within units XX and XXI are consistent with convoluted bedding depicted in the study of soft-sediment deformation by Owen *et al.* (2011). The nonseismic methods for triggering deformation do not fit the depositional or hydrological setting of the study site, suggesting that deformation was likely earthquake induced (Owen *et al.*, 2011).

The interfingering of Px 6 with units XX and XXI combined with its well-sorted grain-size distribution and irregular morphology indicates that the feature was injected into the stratigraphy during the pre-CES earthquake that trig-

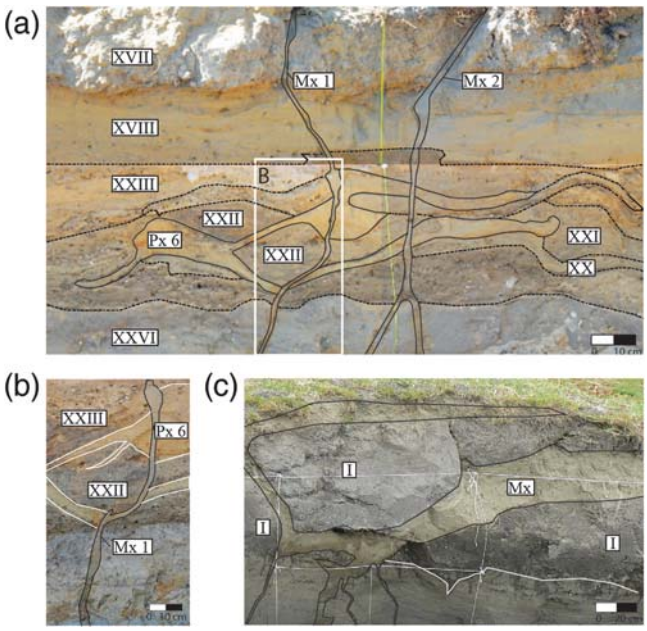

Figure 11. (a) Interpreted field photograph of the north wall of T5 (site 5; Kaiapoi). The CES dike (Mx; outlined in black line) crosscuts the deformed stratigraphy from the trench floor to the surface. Units XX–XXI exhibit soft sediment deformation and are interfingered with Px 6 (outlined in white), interpreted as a pre-CES sandblister. (b) Close-up and interpreted field photograph of the north wall of T5 (site 5). The CES dike (Mx 1) exhibits an oxidized margin from the trench floor into Px 6, suggesting that the CES dike (Mx 1) reactivated the pre-CES sequence dike. (c) Interpreted field photograph of a CES surface blister (adapted with permission from Villamor *et al.*, 2016). The injected liquefied sediment (Mx) crosscuts and fragments the topsoil (I).

gered the soft-sediment deformation. The intrusion of Px 6 around the margins of unit XXII suggests that Px 6 was injected in the near surface causing the former topsoil horizon (XXII) to fragment. This relationship is consistent with the subsurface morphology of a near-surface CES liquefaction injection feature that formed a surface blister and is described by Villamor *et al.* (2016). The CES surface blister described by Villamor *et al.* formed through the near-surface injection of liquefied sediment, which caused the topsoil to fragment and warp upward (Fig. 11c). Px 6 is interpreted as a pre-CES surface blister due to its similar morphology.

No dike feeding Px 6 was observed during excavation; however, the oxidized margins and fine sand surrounding the CES dike extend from the trench floor to the base of the oxidized feature at ~75 cm depth and cannot be traced further. This suggests that the pre-CES dike may have been reactivated by the CES dike (Fig. 11b). Alternatively, an isolated dike that was not intersected within the trench may have fed Px 6. Px 6 interfingers with unit XXIII, indicating that the pre-CES event most likely postdates deposition of this unit and thus the radiocarbon age of A.D. 1297–1381, interpreted as a maximum depositional age (sample R7; Table 1).

The stratigraphy of the south wall appears to exhibit lateral continuity and is undeformed compared with the north wall. This suggests that the deformation was localized and further supports the assertion that Px 6 comprises a localized sandblister (Fig. 10b). No evidence for a buried soil horizon overlying the deformed stratigraphy was observed, suggesting that the unit that the clasts of unit XXI were derived from may have been eroded prior to deposition of units XVII and XVIII (Fig. 10). Units XVII and XVIII do not exhibit deformation, indicating they were likely deposited following the pre-CES earthquake.

Possible Timing of Pre-CES Earthquakes

The approximate timing of the earthquakes forming the pre-CES liquefaction features in Avondale and Kaiapoi may be constrained from crosscutting relationships combined with relative and carbon-14 (^{14}C) ages of the host sediments. It cannot be directly determined whether the pre-CES liquefaction features in Avondale and Kaiapoi formed during the same pre-CES earthquake due to the large age ranges assigned to each feature.

The pre-CES dike, Px 1, identified in T1 (site 1) crosscuts the fluvial sediment to ~105 cm depth, or to ~40 cm if the thickness of the post-CES fill (unit A1) is removed. Px 1 is overlain by unit I. The pre-CES dike, Px 2, in T2 (site 2) crosscuts unit VI to ~65 cm, or ~40 cm without unit A1, and is overlain by unit IV. The proximity of the sites combined with the consistent morphology and similar depths of the pre-CES dikes suggests that these dikes likely formed during the same pre-CES earthquake. The dikes therefore most likely postdate the maximum depositional age of unit III in T1 of A.D. 1321–1453 as derived from radiocabon (sample R1) and predate subdivision of the area in 1960. It cannot be determined whether Px 2 in T2 also formed during this event due to the lack of age constraint.

The pre-CES lateral injection sill (Px 4) identified in T4 (site 4) most likely postdates the radiocarbon age of A.D. 1458–1497 (sample R4; Table 1) interpreted as the maximum depositional age of unit XIII and possibly formed during the 1901 Cheviot earthquake, which is known to have caused liquefaction at the site (Berrill *et al.*, 1994).

The pre-CES sandblow (Px 5) identified in T4 formed at the then-ground surface and thus predates the radiocarbon age of A.D. 1458–1497 interpreted as the maximum depositional age of unit XIII (sample R4; Table 1). No evidence for foreshore sediments was observed in the trench, indicating that the feature postdates the mid-Holocene highstand at ~6500 yr B.P. The preservation of three episodes of liquefaction within the compound sandblow provides evidence for recurrent liquefaction and possible earthquake clustering of sufficient magnitude to trigger repeated liquefaction while the sandblow was exposed at the surface.

Quigley *et al.* (2013) derived a power-law equation for estimating relative $PGA_{7.5}$ based on the variations in relative stratigraphic thickness of units preserved within compound sandblows. The three units identified within the paleosandblow in T4 (Px 5) have maximum stratigraphic thicknesses of

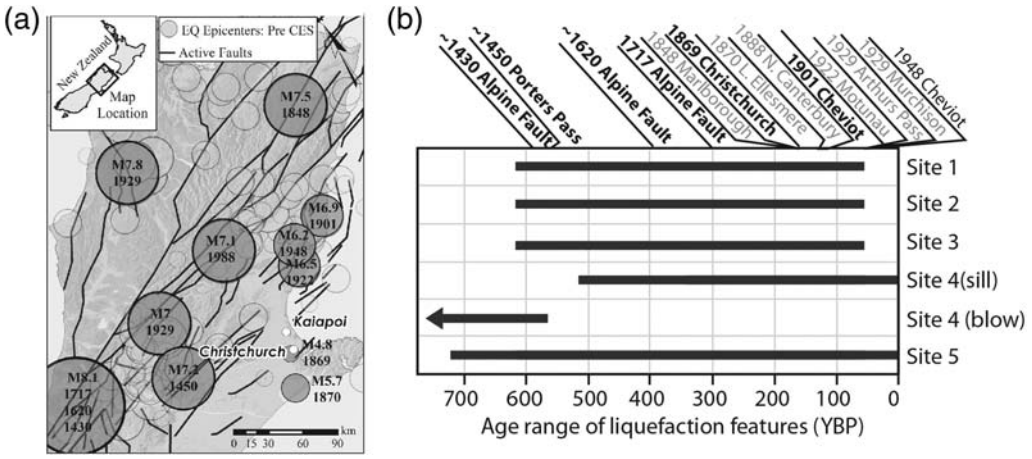

Figure 12. (a) Locations of historic earthquakes plotted in (b) and the known active fault sources that are included in the PGA and backcalculation analysis (fault data from Stirling *et al.*, 2012, and Litchfield *et al.*, 2014, and outlined in Tables 2 and 3). (b) Constrained ages of the pre-CES liquefaction features identified in Avondale, Kaiapoi, and Avonside compared with the chronology of known historic earthquakes (pre-CES) that may have triggered liquefaction in the Canterbury (YBP, years before present). Earthquakes considered likely to trigger liquefaction at the site ($P_L > 15\%$) are indicated in bold.

3.6, 5, and 0.7 cm, respectively (normalized to 0.72, 1.0, and 0.14, respectively). The thicknesses yield crude normalized $PGA_{7.5}$ estimates of the first and third units, being ~70% and ~10% of the $PGA_{7.5}$ of the second event. The lack of a silt lined upper contact on the third unit indicates that the thickness and relative $PGA_{7.5}$ estimates are considered to be minimum for this event.

The presence and stratigraphic relationships of the CES dikes, pre-CES sill, and pre-CES sandblow at site 4 indicate that three separate episodes of liquefaction are preserved within the subsurface. This indicates that the area has been subjected to recurrent liquefaction.

The pre-CES surface blister in T5 (Px 6; Site 5) deforms unit XXIII, indicating that the deformation event likely postdates the maximum depositional age of A.D. 1297–1381 for this unit, as derived from radiocarbon (sample R7; Table 1). The earthquake deformed stratigraphy is overlain by ~0.5 m of fluvial sediment (units XVII and XVIII). It is considered unlikely that ~0.5 m of sediment has accumulated at the site since the 1901 Cheviot earthquake, which is known to have caused liquefaction in the area. The surface blister is therefore considered likely to predate the 1901 Cheviot earthquake. It cannot be determined whether the pre-CES surface sandblister (Px 6) at site 5 formed during the same event as the pre-CES sill (Px 4) or sandblow (Px 5) at site 4 due to the large age ranges assigned to the features and inability to correlate these units stratigraphically.

Potential of Earthquakes on Known Regional Active Faults to Trigger Liquefaction at the Study Sites

The limited historic record of earthquakes within the wider Canterbury region means that the distribution of active faults capable of triggering liquefaction is poorly constrained, and thus the return times of earthquakes triggering liquefaction are largely unknown. Comparison of the timing of the historic and known paleoseismic earthquakes with the age ranges of the pre-CES liquefaction features proves inconclusive in determining the likely causative event due to the large age ranges assigned to each feature (Fig. 12). The large age ranges assigned to the paleoliquefaction features and high number of active faults within the wider Canterbury region create a significant challenge in determining which earthquake sources might have triggered paleoliquefaction at the five sites. For this reason, the potential for known active faults to induce liquefaction at the study sites is assessed from PGA predicted at each site for earthquakes on known active faults and compared with a global liquefaction triggering threshold and from the back-calculated magnitude-bound curves derived by Maurer *et al.* (2015).

The liquefaction susceptibility of the five sites in eastern Canterbury is governed by their hydrologic, geologic, and geomorphic settings. The liquefaction potential of the subsurface sediments generally decreases over time due to aging, including compaction, burial by continued sedimentation, and the precipitation of cements (Seed and Idriss, 1982; Idriss and Boulanger, 2008; Hayati and Andrus, 2009; Maurer *et al.*, 2014). The subsurface sediments at the study sites are likely to have remained saturated since their initial deposition due to the high water tables within Avondale and Kaiapoi. This saturation combined with shallow burial depth and inferred young Holocene age suggests that limited aging has likely occurred. The liquefaction susceptibility of the five sites is therefore likely to have remained relatively unchanged or may have decreased slightly since the pre-CES liquefaction events. The presence of two episodes of liquefaction at sites 1–2 and 5 and preservation of three episodes of liquefaction at site 4 indicate that these areas have remained highly susceptible to liquefaction, and any changes to the liquefiable source sediment during the pre-CES liquefaction events (e.g., compaction) has not had a discernible influence on the liquefaction

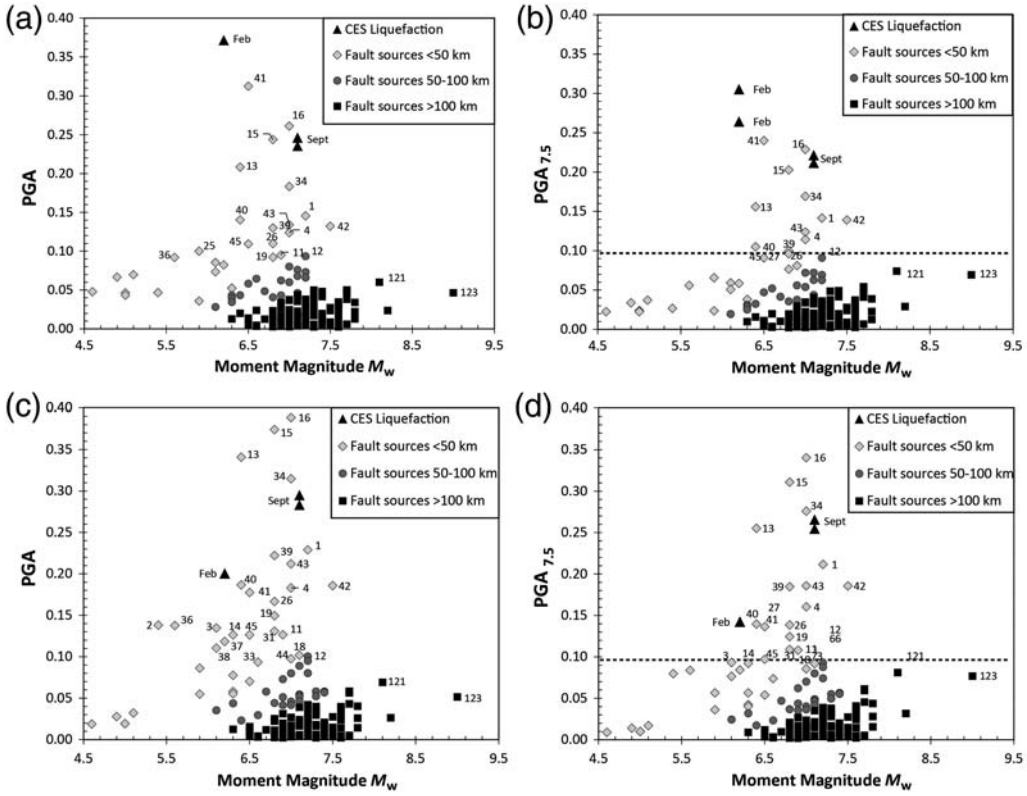

Figure 13. The calculated median PGA generated in (a) Avondale and (c) Kaiapoi for ruptures on active faults within the wider Canterbury region. The calculated median $PGA_{7.5}$ generated in (b) Avondale and (d) Kaiapoi are plotted with the liquefaction triggering threshold of $PGA_{7.5}$ 0.09*g*, as derived by Santucci de Magistris *et al.* (2013). Numbers correspond to faults listed in Table 2, additional data are presented in Ⓔ Table S2.

susceptibility of the sites. The liquefaction-triggering threshold during the paleoearthquakes is therefore likely to be consistent with or slightly lower than that during CES.

Site-Specific Peak Ground Acceleration for Ruptures on Active Faults

Site-specific PGA are derived for Avondale and Kaiapoi from rupture scenarios on the known active faults within the wider Canterbury region using the New Zealand-specific GMPE proposed by Bradley (2013) (Fig. 13). The Bradley GMPE considered four pre-existing global models and was derived from modification of the best-fit Chiou and Youngs (2008) model and calibrated against recorded ground motions in New Zealand. The model computes the median and standard deviation PGA for a given site using the maximum moment magnitude ($M_{w\,max}$), distance of the fault trace to the site (R_{Rup}), predominant rock or soil type, and fault type (i.e., normal, reverse, or strike slip). Estimates of maximum moment magnitude ($M_{w\,max}$) and distances to fault rupture planes (R_{Rup}) were compiled for the wider Canterbury region using Stirling *et al.* (2012) and Litchfield *et al.* (2014) (Table 2). Data on offshore faults were derived from Barnes *et al.* (2011). Site class E soil characteristics (very soft soil) were assumed for both study sites (Standards New Zealand, 2004). Rupture directionality was not considered due to the lack of fault-specific rupture data and because rupture directivity was not explicitly considered during the development of the GMPE.

The median (50th percentile) PGA is plotted for Avondale (Fig. 13a) and Kaiapoi (Fig. 13c) for each rupture scenario. Median PGA values were magnitude weighted ($PGA_{7.5}$) using the magnitude scaling factor proposed by Idriss and Boulanger (2008). $PGA_{7.5}$ represents the equivalent PGA for an M_w 7.5 event and enables direct comparison of ground accelerations irrespective of the earthquake magnitude and distance to epicenter. $PGA_{7.5}$ are plotted for each rupture scenario and compared with the liquefaction triggering threshold of $PGA_{7.5}$ 0.09*g* derived by Santucci de Magistris *et al.* (2013) (Fig. 13). The PGA and $PGA_{7.5}$ of the September 2010 and February 2011 earthquakes are also plotted (Fig. 13). The corresponding fault name, M_w, PGA, and $PGA_{7.5}$ of the faults labeled in Figure 13 are summarized in Table 2. PGA and $PGA_{7.5}$ calculated for all the active faults are summarized in Ⓔ Table S2.

Active faults within 50 km of Avondale that are considered capable of generating $M_w > 6.5$ earthquakes generally plot above the liquefaction triggering threshold of $PGA_{7.5}$ 0.09*g*, indicating that they are likely to trigger widespread liquefaction in Avondale (Fig. 13b). The predicted $PGA_{7.5}$ generated in Avondale from ruptures on the offshore Kaiapoi faults (13), total Kaiapoi faults (15), and the combined Kaiapoi and

Table 2
Active Faults Generating Peak Ground Acceleration (PGA) at the Avondale and Kaiapoi Sites That Exceed the Liquefaction-Triggering Threshold

			Avondale‡		Kaiapoi	
Fault ID*	Fault Name	$M_{w\,max}$†	PGA	Magnitude Normalized PGA ($PGA_{7.5}$)	PGA	$PGA_{7.5}$
1	Ashley	7.4	0.145	0.142	0.229	0.223
2	Ashley mouth	5.4	0.047	0.027	0.138	0.080
3	Ashley part	6.1	0.073	0.051	0.135	0.093
4	Cust	7.2	0.124	0.114	0.183	0.169
10	Offshore Fault VI	6.4	0.043	0.032	0.056	0.042
12	Hororata	7.4	0.093	0.091	0.101	0.098
13	Kaiapoi Offshore	6.4	0.208	0.156	0.341	0.255
14	Kaiapoi Offshore2	6.3	0.052	0.038	0.126	0.092
15	Kaipoi total	6.8	0.244	0.203	0.374	0.311
16	Kaipoi total plus Peg 4 + 4 km	7.0	0.261	0.229	0.389	0.341
18	Kaiwara (south)	7.3	0.076	0.072	0.102	0.097
19	Leithfield	6.8	0.092	0.077	0.150	0.124
26	North Canterbury 1	7.0	0.110	0.096	0.167	0.146
27	North Canterbury 2	6.9	0.049	0.041	0.058	0.050
30	North Canterbury 8	7.3	0.037	0.035	0.042	0.040
33	Omihi	6.7	0.064	0.052	0.094	0.076
34	Pegasus	7.2	0.183	0.169	0.315	0.291
36	Pegasus pup	5.6	0.092	0.056	0.138	0.084
37	Pegasus 3	6.2	0.082	0.059	0.119	0.084
38	Pegasus 4	6.1	0.085	0.059	0.111	0.077
39	Pegasus 5	6.5	0.130	0.100	0.222	0.171
40	Pegasus 6b	6.4	0.140	0.105	0.187	0.140
41	Port Hills	6.5	0.312	0.240	0.178	0.137
42	Porters Pass–Grey	7.7	0.132	0.139	0.186	0.196
43	Springbank	7.2	0.134	0.124	0.212	0.196
44	Springfield	7.1	0.080	0.072	0.098	0.088
45	Waikuku	6.8	0.109	0.091	0.126	0.105
117	Wairarapa–Nicholson	8.3	0.024	0.029	0.026	0.033
121	Alpine (Fiord–Kelly)	8.3	0.060	0.074	0.069	0.085
122	Alpine (Kelly–Tophouse)	7.9	0.006	0.007	0.005	0.006
123	Hikurangi–Wellington	9.0	0.046	0.069	0.051	0.077

Fault names separated with a – refers to segments within a larger fault (i.e., Alpine Fault) and thus the two names denotes the two ends being referred to.

*Fault ID corresponds with ID listed in Ⓔ Table S2 and plotted in Figure 13.

†Fault rupture magnitudes are for maximum rupture scenarios, as listed in Stirling *et al.* (2012).

‡Only active faults with PGA and $PGA_{7.5} > 0.09g$ are listed.

Pegasus faults (16) are similar to that of the September 2010 earthquake, suggesting that ruptures on these faults may trigger moderate-to-severe liquefaction (Fig. 13b). The Alpine fault between Fiordland and Kaniere (121) plots beneath the $PGA_{7.5}$ $0.09g$ threshold for liquefaction but above the threshold value for minor liquefaction in highly susceptible sediments during the CES of $PGA_{7.5}$ $0.06g$ (Quigley *et al.*, 2013). This indicates that the 1717 Alpine fault rupture remains a potentially culpable source for triggering liquefaction in the highly susceptible sediments within Avondale.

In Kaiapoi, the North Canterbury and offshore faults within 50 km of the study sites that are capable of generating $M_w > 5.5$ earthquakes generally plot above the $PGA_{7.5}$ $0.09g$ threshold (Fig. 13d). The higher number of active faults considered capable of triggering reflects the closer proximity of the area to the North Canterbury and offshore fault systems. The $PGA_{7.5}$ calculated for the combined offshore Kaiapoi (15), Kaiapoi and Pegasus combined (16), Kaiapoi offshore (13), and Pegasus (34) faults all exceed the $PGA_{7.5}$ of the September 2010 earthquake, suggesting that they are likely to trigger widespread liquefaction in Kaiapoi (Fig. 13d). The North Canterbury faults, including the Ashley (1), Pegasus (39), Springbank (43), Cust (4), North Canterbury 1 (27), and Porters Pass–Grey (42) all plot between the $PGA_{7.5}$ of the September and February earthquakes, indicating that they are also likely to trigger widespread liquefaction in Kaiapoi (Fig. 13d). The Alpine fault between Fiordland and Kaniere (121) plots at $PGA_{7.5}$ $0.09g$, suggesting that a rupture of this fault length or greater could have triggered liquefaction in Kaiapoi.

Comparison of the site-specific PGA with the liquefaction-triggering threshold indicates that faults proximal (within 50 km) to the study sites are likely to trigger liquefaction. It is possible that the paleoliquefaction features may have formed during prehistoric rupture(s) on these faults. Additionally, many active faults are predicted to generate $PGA_{7.5}$ between the $0.09g$ and $0.06g$ thresholds for liquefaction at both

the Avondale and Kaiapoi sites and thus provide additional possible sources for the paleoliquefaction features (Fig. 13 and Ⓔ Table S2).

Probability of Liquefaction from Magnitude-Bound Curves

The historic earthquakes and active fault sources are plotted in magnitude-bound space with the Maurer *et al.* (2015) probabilistic curves for Avondale (Fig. 14a,b) and Kaiapoi (Fig. 14c,d) to evaluate their probability of triggering liquefaction at the study sites. Maurer *et al.* (2015) derived the back-calculated magnitude-bound curves from liquefaction triggering evaluation, site-response analysis, and ground-motion prediction (Maurer *et al.*, 2015) (see the Ⓔ electronic supplement and Maurer *et al.*, 2015, for further discussion on the framework and use of the derivative curves). Faults with a calculated probability of inducing liquefaction (P_L) $>15\%$ are considered likely to trigger liquefaction at the study sites (Fig. 14). Uncertainties in the probability of liquefaction for each event are quantified by providing minimum and maximum bounds, which approximate 95% confidence bounds (Table 3). The study sites are assigned to a single representative location within Avondale or Kaiapoi to simplify the analysis. This results in a minor miscalculation of the site-to-source distance of >0.5 km, which is within the 95% confidence bounds. The preferred estimate probabilities are indicated in brackets in Table 3.

Rupture magnitudes and site-to-source distances of the large historic earthquakes were derived from paleoseismic studies (Howard *et al.*, 2005) and proposed source models (Doser *et al.*, 1999). Empirical site-to-source distance conversions are applied for historic earthquakes with proposed epicentral locations (Scherbaum *et al.*, 2004). Magnitude estimates and site-to-source distances of the active faults are adopted from Stirling *et al.* (2012) and Barnes *et al.* (2011), where a maximum rupture scenario is considered. The rupture magnitudes and site-to-source distances of the active faults are assigned uncertainties of $\pm 0.36\, M_w$ and ± 4 km, which represent approximate 95% confidence bounds. It is acknowledged that a fully probabilistic model would consider the range of earthquake magnitudes, recurrence interval, and possible segmentation of each fault; however, these data are not provided in the New Zealand seismic-hazard model (Stirling *et al.*, 2012) and is considered to be beyond the scope of this study.

In Avondale, the Alpine fault rupture of $M_w \sim 8.1$ in 1717 and the $M_w \sim 7.2$ Porters Pass earthquake in ~1450 have the highest probabilities of triggering liquefaction for the known historic earthquakes (32% and 19%, respectively; Fig. 14a,b). The 1869 $M_w \sim 4.8$ Christchurch earthquake has a preferred P_L of 7%; however, it has an upper-bound estimate of $P_L = 43\%$, which reflects the large uncertainty in the location of the fault rupture. The upper-bound estimate indicates that the earthquake may have triggered liquefaction within Avondale. The active faults within 50 km of Avondale and capable of generating $M_w > 6.5$ earthquakes generally plot at $P_L \geq 15\%$ and thus are considered capable of triggering liquefaction. The Kaiapoi–Pegasus, Kaiapoi, Pegasus, Kaiapoi Offshore, and Ashley faults all have $P_L > 70\%$, indicating that earthquakes on these faults have a high probability of triggering liquefaction in Avondale (Table 3). The Kaiapoi–Pegasus fault (16) has a P_L similar to the Port Hills fault (41), which ruptured during the February 2011 earthquake (P_L of 94% and 95%), indicating that liquefaction induced during a rupture on the Pegasus fault is likely to be similar to that observed in Avondale during the February 2011 earthquake.

In Kaiapoi, the 1717 $M_w \sim 8.1$ Alpine fault rupture ($P_L = 35\%$), ~1450 Porters Pass earthquake ($P_L = 24\%$), and 1901 Cheviot earthquake ($P_L = 23\%$) have credible potential for inducing liquefaction. The P_L estimate for the 1901 Cheviot earthquake is consistent with the observed liquefaction during this event (Berrill *et al.*, 1994). Active faults within 50 km of the study sites that are capable of generating $M_w > 5.5$ earthquakes generally plot at $P_L > 15\%$ and are therefore considered likely to trigger liquefaction. The Pegasus, Kaiapoi–Pegasus, Kaiapoi Offshore, Kaiapoi, Springbank, Porters Pass–Grey, Ashley, Cust, and Waikuku faults have $P_L > 70\%$, indicating that these faults have a high probability of triggering liquefaction. It is likely that liquefaction during a maximum rupture on the Alpine fault ($P_L = 35\%$) would be similar to that observed during the 1901 Cheviot earthquake ($P_L = 23\%$).

The back-calculated magnitude-bound procedure indicates that historic ruptures on the Alpine fault and Porters Pass fault, and ruptures predicted for active faults within the North Canterbury and offshore fault systems, have a high probability of triggering liquefaction at the study sites. The results are generally in agreement with those identified from comparison of the site-specific PGA and liquefaction-triggering threshold. Combining the backcalculation approach with the PGA and $PGA_{7.5}$ derived from the GMPE proves effective in determining the active faults capable of triggering liquefaction at the study sites and thus also may have triggered paleoliquefaction.

Implications for Paleoseismic Studies and Future Land Use

The CES highlights the severe damage and disruption to land, infrastructure, and lifelines that can result from liquefaction (Cubrinovski *et al.*, 2010, 2011; Hughes *et al.*, 2015). Because of the limited historic record, the return times of liquefaction-triggering earthquakes within the city are uncertain, and thus the liquefaction hazard posed by future earthquakes is largely unknown. Combining the backcalculation approach with the PGA and $PGA_{7.5}$ derived from the GMPE proves effective in determining the active faults capable of triggering liquefaction at the study sites. The large number of active faults within the wider Canterbury region that are anticipated to trigger liquefaction at the Kaiapoi and Avon-

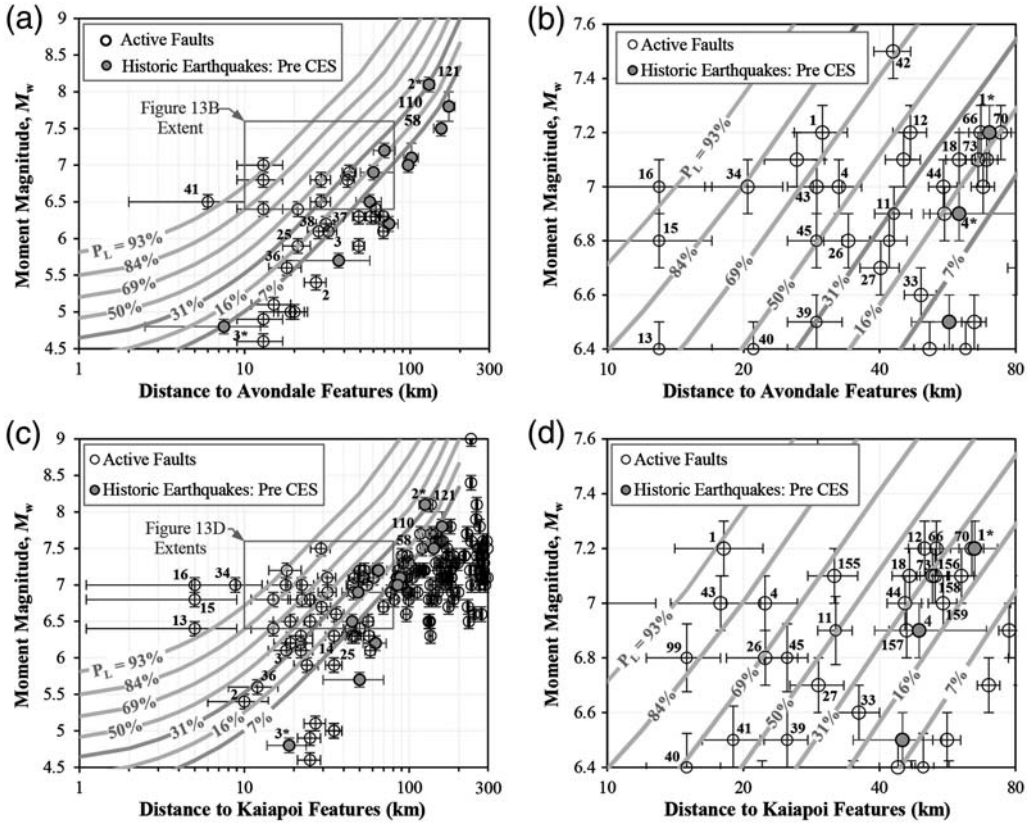

Figure 14. Magnitude-bound curves indicating the probability of known historic earthquakes (pre-CES) and active faults within the wider Canterbury region to induce liquefaction ($P_L > 15\%$) within (a) Avondale and (c) Kaiapoi. Subsets of the (b) Avondale and (d) Kaiapoi data are shown in greater detail. Numbers corresponding with fault codes are listed in Table 3.

dale sites highlights the need for local authorities to assess the liquefaction hazard for present and future developments, both in Christchurch and in other seismically active areas that are underlain by sediments highly susceptible to liquefaction.

The presence of pre-CES liquefaction in Avondale and Kaiapoi indicates that the eastern Canterbury region had liquefied prior to the CES and 1901 Cheviot earthquake. The inferred pre-1960 age of the features in Avondale indicates that residential development took place on top of sediments that contained geologic evidence for liquefaction. The identification of three generations of liquefaction at site 2 in Kaiapoi (CES, likely 1901, and pre-A.D. 1497) indicates that the area has been subjected to recurrent liquefaction. Additionally, the preservation of three episodes of liquefaction within the pre-CES compound sandblow provides evidence of possible earthquake clustering prior to the CES clustering. Development in Kaiapoi therefore took place on sediments that had historically liquefied and contained evidence for prehistoric earthquake clustering. The high number of active faults in North Canterbury and offshore that are considered capable of triggering liquefaction in Kaiapoi, combined with the identification of pre-CES liquefaction, confirms that the area is highly susceptible to liquefaction.

The presence of both pre-CES and CES liquefaction in the five trenches indicates that the same areas reliquefy during subsequent earthquake events. The documentation of pre-CES features also highlights the potential of paleoliquefaction investigations, in addition to geotechnical data, to contribute to land-use planning.

Conclusions

The CES liquefaction features documented at the five sites consist of liquefaction dikes and sills composed of well-sorted fine sand and silt that lacks the oxidation and mottling developed in the surrounding sediment. The dikes all exhibit a similar subvertical and planar geometry and increase in width with depth.

Pre-CES liquefaction features identified in the trenches include dikes at sites 1 and 2, possible pre-CES injection sill at site 3, a sill and compound sandblow at site 4, and a sandblister at site 5. Crosscutting relationships combined with ^{14}C dating indicate that the Avondale event most likely occurred between 1321 and 1960. The sill identified at site 4 in Kaiapoi postdates 1458 and likely formed during the 1901 earthquake, whereas the sandblow most likely predates 1458. The sandblister at site 5 likely formed between 1297 and 1901. The presence of pre-CES liquefaction confirms that moderate-to-large earthquakes occurred in eastern Canterbury prior to the CES and 1901 Cheviot earthquake.

Table 3
Potential of Known Historic Earthquakes and Active Faults to Induce Liquefaction in Avondale and Kaiapoi

Fault Code*	Historic Earthquakes and Active Faults	M_w†	Computed P_L: 95% Confidence Bounds (Preferred Estimate)‡	
			Avondale	Kaiapoi
1*	1450 Porters Pass	7.2	6%–42% (19%)	10%–56% (24%)
2*	1717 Alpine	8.1	15%–50% (32%)	18%–53% (35%)
3*	1869 Christchurch	4.8	1%–43% (7%)	1%–2% (1%)
4*	1901 Cheviot	6.9	2%–34% (13%)	4%–50% (23%)
41	Port Hills	6.5	72%–99% (95%)	23%–87% (62%)
16	Kaiapoi–Pegasus	7.0	73%–99% (94%)	93%–99% (99%)
15	Kaiapoi	6.8	62%–99% (89%)	88%–99% (99%)
34	Pegasus	7.0	51%–96% (83%)	85%–99% (98%)
13	Kaiapoi Offshore	6.4	35%–95% (74%)	71%–99% (95%)
1	Ashley	7.2	42%–92% (73%)	70%–99% (92%)
42	Porters Pass–Grey	7.5	41%–93% (70%)	63%–97% (87%)
43	Springbank	7.0	30%–87% (64%)	58%–98% (87%)
4	Cust	7.0	25%–83% (56%)	46%–95% (77%)
45	Waikuku	6.8	20%–80% (50%)	54%–98% (86%)
12	Hororata	7.2	18%–73% (45%)	15%–69% (40%)
40	Pegasus 6b	6.4	19%–79% (45%)	28%–92% (67%)
26	North Canterbury Shelf 1	6.8	14%–70% (40%)	32%–90% (69%)
11	Offshore Fault IV	6.9	10%–61% (30%)	20%–81% (50%)
39	Pegasus 5	6.4	12%–66% (30%)	13%–74% (40%)
19	Leithfield	6.8	7%–56% (26%)	27%–87% (60%)
27	North Canterbury Shelf 2	6.7	6%–52% (23%)	15%–74% (42%)
121	Alpine: Fiordland to Kaniere	8.1	7%–46% (23%)	10%–50% (29%)
18	Kaiwara South	7.1	6%–51% (22%)	15%–68% (38%)
44	Springfield	7.0	6%–50% (21%)	11%–65% (33%)
73	Waitohi	7.1	4%–44% (17%)	10%–60% (31%)
70	Torlesse	7.2	4%–42% (16%)	6%–53% (25%)
30	North Canterbury 8-10	7.1	3%–40% (15%)	6%–50% (22%)
110	Clarence Northeast	7.7	2%–32% (12%)	4%–40% (16%)
33	Omihi	6.6	2%–31% (10%)	6%–54% (24%)
36	Pegasus pup	5.6	1%–42% (10%)	4%–71% (27%)
3	Ashley Partial	6.1	1%–31% (8%)	16%–73% (35%)
14	Kaiapoi Offshore 2	6.3	1%–15% (3%)	10%–71% (35%)
2	Ashley Mouth	5.4	1%–8% (1%)	3%–70% (24%)

*Fault ID corresponds with ID listed in Ⓔ Table S2 and plotted in Figure 14.
†Fault rupture magnitudes are for maximum rupture scenarios, as listed in Stirling *et al.* (2012).
‡Only historic earthquakes and active faults with credible potential for inducing liquefaction ($P_L \geq 15\%$) at Avondale or Kaiapoi are listed.

The site-specific PGA indicates that many faults within 50 km of the study sites have the potential to trigger widespread liquefaction and may have formed the pre-CES features. Additionally, many faults have the potential to trigger minor-to-moderate liquefaction in both Avondale and Kaiapoi.

The magnitude-bound backcalculation indicates that the 1717 $M_w \sim 8.1$ Alpine fault and $\sim$1450 $M_w \sim 7.2$ Porters Pass earthquakes are highly likely to have triggered liquefaction in Avondale and Kaiapoi. Additionally, the Pegasus, Kaiapoi, Kaiapoi–Pegasus, and Ashley faults are considered highly likely to trigger liquefaction in Avondale ($P_L > 70\%$) and may have formed the paleoliquefaction features. In Kaiapoi, the Pegasus, Kaiapoi–Pegasus, Kaiapoi Offshore, Waikuku, Springbank, Porters Pass–Grey, Ashley, and Cust faults are considered likely to trigger severe liquefaction ($P_L > 70\%$).

Combining the backcalculation approach with the PGA and $PGA_{7.5}$ derived from the GMPE proves effective in determining active faults that are capable of triggering liquefaction at the study sites and are thus capable of triggering liquefaction in the future. The results are generally in agreement as to which faults are likely to have triggered liquefaction in Avondale and/or Kaiapoi.

Data and Resources

Information on the purchasing of upward of 7000 residential properties in eastern Christchurch and Kaiapoi was obtained from http://cera.govt.nz/news/2012/flat-land-residential-zoning-now-complete-18-may2012 (last accessed June 2015). The history of the Avon River, including information on the straightening of the river, was obtained from http://christchurchcitylibraries.com/Heritage/Chronology/Year/1950.asp (last accessed June 2015).

The high-resolution post 22 February 2011 aerial photographs were obtained from the LINZ Data Service (https://koordinates.com/layer/3185-christchurch-post-earthquake-aerial-photos-24-feb-2011/, last accessed June 2015). The peak ground acceleration of the CES earthquakes were obtained from the Canterbury Geotechnical Database website https://canterburygeotechnicaldatabase.projectorbit.com (last accessed June 2015). The CPT and fault source data used in this article were obtained from the published sources listed in the references.

Acknowledgments

We thank Martitia Tuttle, Peter Almond, and Catherine Reid for their discussions that aided the interpretation of the pre-CES liquefaction features. We also thank Sjoerd van Ballegooy for his enthusiastic critiques of our research and his assistance with processing and interpreting the cone penetration test (CPT) data. This work was funded by an EQC Capability Fund and the University of Canterbury Mason Trust Fund. R. Green and B. Maurer's efforts on this study were supported by the U.S. National Science Foundation (NSF) Grants CMMI-1407428 and CMMI-1435494 and U.S. Geological Survey (USGS) Grants G12AP20002 and G14AP00046. However, any opinions, findings, and conclusions or recommendations expressed in this article are those of the authors and do not necessarily reflect the views of EQC Capability Fund, the University of Canterbury Mason Trust Fund, NSF, or USGS.

References

Barnes, P. M., C. Castellazzi, A. Gorman, and S. Wilcox (2011). Submarine faulting beneath Pegasus Bay, offshore Christchurch, Wellington, *Report WLG2011-28*, National Institute of Water and Atmospheric Research Ltd (NIWA), 46 pp.

Bastin, S., M. C. Quigley, and K. Bassett (2015). Paleo-liquefaction in Christchurch, New Zealand, *Geol. Soc. Am. Bull.* **127,** nos. 9/10, 1348–1365.

Berrill, J. B., P. C. Mulqueen, and E. T. C. Ooi (1994). Liquefaction at Kaiapoi in the 1901 Cheviot, New Zealand, earthquake, *Bull. New Zeal. Soc. Earthq. Eng.* **24,** no. 3, 178–189.

Bradley, B. (2013). A New Zealand-specific pseudospectral acceleration ground-motion prediction equation for active shallow crustal earthquakes based on foreign models, *Bull. Seismol. Soc. Am.* **103,** no. 3, 1801–1822.

Brown, L. J., and J. H. Weeber (1992). Geology of the Christchurch urban area, *Institute of Geological and Nuclear Sciences Geological Map 1*, Institute of Geological and Nuclear Sciences Limited, Lower Hutt, New Zealand, scale 1:25,000, 1 sheet + 105 pp.

Chiou, B. S. J., and R. R. Youngs (2008). An NGA model for the average horizontal component of peak ground motion and response spectra, *Earthq. Spectra* **24,** 173–215.

Christchurch Engineering Lifelines Group (1997). Risks and realities: A multi-disciplinary approach to the vulnerability of lifelines to natural hazards, *Report of the Christchurch Engineering Lifelines Group*, Centre for Advanced Engineering, Christchurch, New Zealand.

Clough, B. (2005). Christchurch liquefaction study: Stage IV (addendum report), *Environment Canterbury Report U04/25/2*, Beca, Carter, Hollings and Ferner Ltd, Christchurch, New Zealand.

Counts, R. C., and S. F. Obermeier (2012). Subtle seismic signatures, using small-scale features and ground fractures as indicators of paleoseismicity, in *Recent Advances in North American Paleoseismology and Neotectonics East of the Rockies*, R. T. Cox, M. P. Tuttle, O. Boyd, and J. Locat (Editors), *Spec. Pap. Geol. Soc. Am.*, Vol. 493, 203–219.

Cowie, C. A. (1957). *Floods in New Zealand 1920–1953, with Notes on Some Earlier Floods*, The Soil Conservation and Rivers Control Council, Wellington, New Zealand.

Cubrinovski, M., J. D. Bray, M. Taylor, S. Giorgini, B. Bradley, L. Wotherspoon, and J. Zupan (2011). Soil liquefaction effects in the central business district during the February 2011 Christchurch earthquake, *Seismol. Res. Lett.* **82,** no. 6, 893–904.

Cubrinovski, M., R. A. Green, J. Allen, S. Ashford, B. Bradley, E. Bowman, B. Cox, T. Hutchinson, E. Kavazanjian, R. Orense, *et al.* (2010). Geotechnical reconnaissance of the 2010 Darfield (Canterbury) earthquake, *Bull. New Zeal. Soc. Earthq. Eng.* **43,** no. 4, 243–320.

Doser, D. I., T. H. Webb, and D. E. Mauder (1999). Source parameters of large historical (1918–1962) earthquakes, South Island, New Zealand, *Geophys. J. Int.* **139,** no. 3, 769–794.

Downes, G., and M. Yetton (2012). Pre-2010 historical seismicity near Christchurch, New Zealand: The 1869 M_w 4.7–4.9 Christchurch and 1870 M_w 5.6–5.8 Lake Ellesmere earthquakes, *New Zeal. J. Geol. Geophys.* **55,** no. 3, 199–205.

Elder, D. M., I. F. McCahon, and M. D. Yetton (1991). The earthquake hazard in Christchurch: A detailed evaluation, *Research Report to the EQC*, Soils and Foundations Ltd., Christchurch, New Zealand.

Forsyth, P. J., D. J. A. Barrell, and R. Jongens (compilers) (2008). *Geology of the Christchurch area*, Institute of Geological & Nuclear Sciences, GNS Science, Lower Hutt, scale 1:250,000, geological map 16, 67 pp. + 1 folded map.

Green, R. A., S. F. Obermeier, and S. M. Olson (2005). Engineering geologic and geotechnical analysis of paleoseismic shaking using liquefaction effects: Field examples, *Eng. Geol.* **76,** 263–293.

Griffiths, G. A. (1979). Recent sedimentation history of the Waimakariri River, New Zealand, *J. Hydrol.* **18,** 6–28.

Hawkins, D. N. (1957). *Beyond the Waimakariri: A Regional History*, Whitcombe and Tombs, Christchurch, New Zealand.

Hayati, H., and R. D. Andrus (2009). Updated liquefaction resistance correction factors of aged sands, *J. Geotech. Geoenviron. Eng.* **135,** no. 11, 1683–1692.

Howard, M., A. Nicol, J. Campbell, and J. R. Pettinga (2005). Holocene paleoearthquakes on the strike-slip Porters Pass fault, Canterbury, New Zealand, *New Zeal. J. Geol. Geophys.* **48,** 59–74.

Hughes, M. W., M. C. Quigley, S. van Ballegooy, B. L. Deam, B. A. Bradley, and D. E. Hart (2015). The sinking city: Earthquakes increase flood hazard in Christchurch, New Zealand, *GSA Today* **25,** no. 3, 4–10.

Idriss, I. M., and R. W. Boulanger (2008). *Soil Liquefaction during Earthquakes*, Monograph Series, Earthquake Engineering Research Institute, Oakland, California.

Litchfield, N. J., R. J. van Dissen, R. Sutherland, P. M. Barnes, S. C. Cox, R. Norris, R. J. Beavan, R. M. Langridge, P. Villamor, K. R. Berryman, *et al.* (2014). A model of active faulting in New Zealand, *New Zeal. J. Geol. Geophys.* **57,** no. 1, 32–56.

Logan, R. (2008). *Waimakariri: An Illustrated History*, Phillips and King, Christchurch, New Zealand.

Maurer, B. W., R. A. Green, M. Cubrinovski, and B. A. Bradley (2014). Assessment of aging correction factors for liquefaction resistance at sites of recurrent liquefaction: A study of the Canterbury (NZ) earthquake sequence, *Proc. 10th National Conference on Earthquake Engineering (10NCEE)*, Anchorage, Alaska, 21–25 July 2014.

Maurer, B. W., R. A. Green, M. C. Quigley, and S. Bastin (2015). Development of magnitude-bound relations for paleoliquefaction analyses: New Zealand case study, *Eng. Geol.* **197** 253–266.

McCormac, F. G., A. G. Hogg, P. G. Blackwell, C. E. Buck, T. F. G. Higham, and P. J. Reimer (2004). SHCAL04 Southern Hemisphere calibration, 0-11.0 Cal kyr BP, *Radiocarbon* **46,** no. 3, 1087–1092.

Obermeier, S. F. (1996). Use of liquefaction-induced features for paleoseismic analysis—An overview of how seismic liquefaction features can be distinguished from other features and how their regional distribution and properties of source sediment can be used to infer the location and strength of Holocene paleo-earthquakes *Eng. Geol.* **44,** 1–76.

Obermeier, S. F. (1998). Liquefaction evidence for strong earthquakes of Holocene and latest Pleistocene ages in the states of Indiana and Illinois, USA, *Eng. Geol.* **50,** 227–254.

Obermeier, S. F., S. M. Olson, and R. A. Green (2005). Field occurrences of liquefaction-induced features: A primer for engineering geologic analysis of paleoseismic shaking, *Eng. Geol.* **76,** 209–234.

Olson, S. M., R. A. Green, and S. F. Obermeier (2005). Revised magnitude bound relation for the Wabash Valley seismic zone of the central United States, *Seismol. Res. Lett.* **76,** no. 6, 756–771.

Owen, G., M. Moretti, and P. Alfaro (2011). Recognising triggers for soft-sediment deformation: Current understanding and future directions, *Sediment. Geol.* **235,** 133–140.

Papathanassiou, G., S. Pavlides, B. Christaras, and K. Pitilakis (2005). Liquefaction case histories and empirical relations of earthquake magnitude versus distance from the broader Aegean region, *J. Geodyn.* **40,** nos. 2/3, 257–278.

Parker, M., and D. Steenkamp (2012). The economic impact of the Canterbury earthquakes, *Reserve Bank New Zeal. Bull.* **75,** no. 3, 13–25.

Pettinga, J. R., M. D. Yetton, R. J. Van Dissen, and G. Downes (2001). Earthquake source identification and characteristics for the Canterbury region, South Island, *Bull. New Zeal. Soc. Earthq. Eng.* **34,** no. 4, 282–317.

Pirrotta, C., M. S. Barbano, P. Guarnieri, and F. Gerardi (2007). A new dataset and empirical relationships between magnitude/intensity and epicentral distance for liquefaction in central-eastern Sicily, *Ann. Geophys.* **50,** no. 6, 763–774.

Quigley, M. C., S. Bastin, and B. A. Bradley (2013). Recurrent liquefaction in Christchurch New Zealand, during the Canterbury earthquake sequence, *Geology* **41,** no. 5, 419–422.

Reid, C. M., N. K. Thompson, J. R. M. Irvine, and T. E. Laird (2012). Sand volcanoes in the Avon-Heathcote estuary produced by the 2010–2011 Christchurch earthquakes: Implications for geological preservation and expression, *New Zeal. J. Geol. Geophys.* **55,** no. 3, 249–254.

Santucci de Magistris, F., G. Lanzano, G. Forte, and G. Fabbrocino (2013). A database for PGA threshold in liquefaction occurrence, *Soil Dynam. Earthq. Eng.* **54,** 17–19.

Scherbaum, F., J. Schmedes, and F. Cotton (2004). On the conversion of source-to-site distance measures for extended earthquake source models, *Bull. Seismol. Soc. Am.* **94,** no. 3, 1053–1069.

Seed, H. B., and I. M. Idriss (1982). *Ground Motions and Soil Liquefaction during Earthquakes*, Monograph Series, Earthquake Engineering Research Institute, Berkeley, California.

Sims, J. D., and C. D. Garvin (1995). Recurrent liquefaction induced by the 1989 Lorna Prieta earthquake and 1990 and 1991 aftershocks: Implications for paleoseismicity studies, *Bull. Seismol. Soc. Am.* **85,** no. 1, 51–65.

Standards New Zealand (2004). *Structural Design Actions Part 5: Earthquake Actions*, NZS.1170.5, Standard New Zealand, Wellington, New Zealand.

Stirling, M., G. McVerry, M. Gerstenberger, N. Litchfield, R. Van Dissen, K. Berryman, P. Barnes, L. Wallace, P. Villamor, R. Langridge, *et al.* (2012). National seismic hazard model for New Zealand: 2010 update, *Bull. Seismol. Soc. Am.* **102,** no. 4, 1514–1542.

Stirling, M., M. Yetton, J. Pettinga, K. R. Berryman, and G. L. Downes (1999). Probabilistic seismic hazard assessment and earthquake scenarios for the Canterbury region, and historic earthquakes in Christchurch. Stage 1 (Part B) of Canterbury Regional Council's earthquake hazard and risk assessment study, *Institute of Geological and Nuclear Sciences Client Report 1999/53*, GNS Science, Lower Hutt, New Zealand.

Sutherland, R., D. Eberhart-Phillips, R. A. Harris, T. A. Stern, R. J. Beavan, S. M. Ellis, S. A. Henrys, S. C. Cox, R. J. Norris, K. R. Berryman, *et al.* (2007). Do great earthquakes occur on the Alpine fault in central South Island, New Zealand? in *A Continental Plate Boundary: Tectonics at South Island, New Zealand*, D. A. Okaya, T. A. Stern, and F. J. Davey (Editors), Geophysical Monograph 175, American Geophysical Union, Washington D.C., 235–251.

Tuttle, M. P. (2001). The use of liquefaction features in paleoseismology: Lessons learned in the New Madrid seismic zone, central United States, *J. Seismol.* **5,** 361–380.

Tuttle, M. P., and G. M. Atkinson (2010). Localization of large earthquakes in the Charlevoix seismic zone, Quebec, Canada during the past 10,000 years, *Seismol. Res. Lett.* **81,** no. 1, 18–25.

Tuttle, M., and N. Barstow (1996). Liquefaction-related ground failure: A case study in the New Madrid seismic zone, central United States, *Bull. Seismol. Soc. Am.* **86,** no. 3, 636–645.

Tuttle, M. P., and R. Hartleb (2012). CEUS Paleo-liquefaction database, uncertainties associated with paleo-liquefaction data, and guidance for seismic source characterization: Central and eastern United States seismic source characterization for nuclear facilities, Appendix E, *NUREG-2115*, Vol. 5, Appendixes C–F, U.S. Department of Energy (DOE), U.S. Nuclear Regulatory Commission (NRC), and Electric Power Research Institute (EPRI), Palo Alto, California, Accession No. ML12048A859.

Tuttle, M. P., E. S. Schweig, J. D. Sims, R. H. Lafferty, L. W. Wolf, and M. L. Haynes (2002). The earthquake potential of the New Madrid seismic zone, *Bull. Seismol. Soc. Am.* **92,** no. 6, 2080–2089.

van Breemen, N., and P. Buurman (2002). *Soil Formation*, Second Ed., Kluwer Academic Publishers, Dordrecht, The Netherlands.

Villamor, P., P. Almond, M. Tuttle, M. Giona-Bucci, R. M. Langridge, K. Clark, W. Ries, S. H. Bastin, A. Eger, M. Vandergoes, *et al.* (2016). Liquefaction features produced by the 2010–2011 Canterbury earthquake sequence in 995 southwest Christchurch, New Zealand and preliminary assessment of paleoliquefaction features, *Bull. Seismol. Soc. Am.* **106,** no. 4, doi: 10.1785/0120150223.

Wilson, J. (1989). *Christchurch Swamp to City: A Short History of the Christchurch Drainage Board 1875–1989*, Christchurch Drainage Board, Christchurch, New Zealand.

Wood, P. (1993). *Kaiapoi: A Search for Identity*, Waimakariri District Council, Rangiora, New Zealand.

Wotherspoon, L. M., M. J. Pender, and R. P. Orense (2012). Relationship between observed liquefaction at Kaiapoi following the 2010 Darfield earthquake and former channels of the Waimakariri River, *Eng. Geol.* **125,** 45–55.

Department of Geological Sciences
University of Canterbury
Private Bag 4800
Christchurch, New Zealand
(S.H.B., K.B., M.C.Q., D.J.)

Department of Civil and Environmental Engineering
Virginia Tech
120-B Patton Hall
Blacksburg, Virginia 24061
(B.M., R.A.G.)

Department of Civil and Natural Resource Engineering
University of Canterbury
Private Bag 4800
Christchurch, New Zealand
(B.B.)

Manuscript received 10 March 2016;
Published Online 9 June 2016